doi:10.1016/j.jmb.2004.12.031 *J. Mol. Biol.* (xxxx) **xx**, 1–23

JMB

Available online at www.sciencedirect.com

SCIENCE @ DIRECT®

ELSEVIER

Refined Structure of the Nicotinic Acetylcholine Receptor at 4 Å Resolution

Nigel Unwin

MRC Laboratory of Molecular Biology, Hills Road, Cambridge CB2 2QH, UK

We present a refined model of the membrane-associated *Torpedo* acetylcholine (ACh) receptor at 4 Å resolution. An improved experimental density map was obtained from 342 electron images of helical tubes, and the refined structure was derived to an *R*-factor of 36.7% (R_{free} 37.9%) by standard crystallographic methods, after placing the densities corresponding to a single molecule into an artificial unit cell. The agreement between experimental and calculated phases along the helical layer-lines was used to monitor progress in the refinement and to give an independent measure of the accuracy. The atomic model allowed a detailed description of the whole receptor in the closed-channel form, including the ligand-binding and intracellular domains, which have not previously been interpreted at a chemical level. We confirm that the two ligand-binding α subunits have a different extended conformation from the three other subunits in the closed channel, and identify several interactions on both pairs of subunit interfaces, and within the α subunits, which may be responsible for their "distorted" structures. The ACh-coordinating amino acid side-chains of the α subunits are far apart in the closed channel, indicating that a localised rearrangement, involving closure of loops B and C around the bound ACh molecule, occurs upon activation. A comparison of the structure of the α subunit with that of AChBP having ligand present, suggests how the localised rearrangement overcomes the distortions and initiates the rotational movements associated with opening of the channel. Both vestibules of the channel are strongly electronegative, providing a cation-stabilising environment at either entrance of the membrane pore. Access to the pore on the intracellular side is further influenced by narrow lateral windows, which would be expected to screen out electrostatically ions of the wrong charge and size.

Keywords: acetylcholine receptor; ion channel; refinement; electron microscopy

Introduction

The nicotinic ACh receptor is a member of the pentameric "Cys-loop" superfamily of transmitter-gated ion channels, which includes neuronal ACh receptors, $GABA_A$ receptors, $5\text{-}HT_3$ receptors and glycine receptors.[1–5] The channel is found in high concentrations at the nerve–muscle synapse, where it mediates fast chemical transmission of electrical signals in response to ACh released from the nerve terminal into the synaptic cleft. It is a large (290 kDa) glyco-protein, assembled from a ring of homologous subunits (α, γ, α, β, δ) and divided into three domains: a large N-terminal extracellular ligand-binding domain, a membrane-spanning pore, and a smaller intracellular domain, giving it a total length of about 160 Å normal to the membrane plane. The ligand-binding domain shapes a long, ∼20 Å diameter central vestibule and has two binding sites for ACh, which are about 40 Å from the membrane surface on opposite sides of the pore. The pore makes a narrow water-filled path across the membrane and contains the gate, which opens when ACh occupies both binding sites. The intracellular domain shapes another, smaller vestibule, having narrow lateral openings for the ions.

The receptor subunits in the ligand-binding

Abbreviations used: ACh, acetylcholine; AChBP, ACh-binding protein; MIR, main immunogenic region.

E-mail address of the author mas@mrc-lmb.cam.ac.uk

domain are each organised around two sets of β-sheets packed into a curled β-sandwich and joined through the disulphide bridge forming the Cys loop, as was shown by the structure of the closely related soluble protein, AChBP.[6] The ACh-binding sites lie at the α–γ and α–δ subunit interfaces, and are contributed mainly by residues from loops A, B and C, connecting β-strands in the α subunits.[7–9] The subunits in the membrane-spanning domain are each made from four α-helical segments (M1–M4).[10] The helical segments are arranged symmetrically, forming an inner ring of helices (M2), which shape the pore, and an outer shell of helices (M1, M3 and M4), which coil around each other and shield the inner ring from the lipids. In the closed channel, the inner ring of helices come together near the middle of the membrane to make a constricting hydrophobic girdle, which constitutes an energetic barrier to ion permeation[11,12] and may function as the gate of the channel.[10,13] The subunits in the intracellular domain each contribute one α-helix (part of the M3–M4 loop), which together make the wall of the vestibule.[14]

Insight into the structural mechanism of gating has been obtained by electron microscopical experiments on helical tubes grown from *Torpedo* postsynaptic membranes,[15,16] using a rapid spray-freezing technique to mimic the synaptic release of ACh and trap the open-channel form.[17] These experiments showed that binding of ACh initiates two interconnected events in the ligand-binding domain. One is a local disturbance in the region of the ACh-binding sites, and the other a larger-scale conformational change, involving rotational movements predominantly in the two α subunits. The inner M2 helices also change their configuration in response to ACh, widening the lumen of the pore at the middle of the membrane. Higher resolution studies of the extended conformational change[18] and of the structure in the membrane[10] suggested a simplified mechanical model for the channel opening mechanism, whereby ACh triggers rotations of the inner β-sheets of the α subunits and the twisting movement, communicated through the inner helices, breaks the gate apart.

In addition to the structural details, summarised above, the roles played by individual amino acid residues in determining the ligand-binding, gating and cation-conduction properties of the ACh receptor have been extensively characterised by chemical labelling and by site-directed mutagenesis experiments combined with electrophysiological study of function.[19–28] Other experiments of this kind, performed on GABA$_A$, glycine, 5-HT$_3$ and neuronal α7 receptors constitute a wealth of complementary information.

We report here a preliminary three-dimensional framework for relating these biochemical and physiological data, based on refinement of a 4 Å structure obtained from electron images of the tubular *Torpedo* membranes frozen in a near-physiological ionic environment.[10] The refined model enables a detailed description of the whole receptor in the closed-channel form, including the ligand-binding region and vestibular entrances, which have not previously been interpreted at a chemical level. We confirm that the two ligand-binding α subunits have a different extended conformation from the three other subunits in the closed-channel form of the receptor,[18] and identify

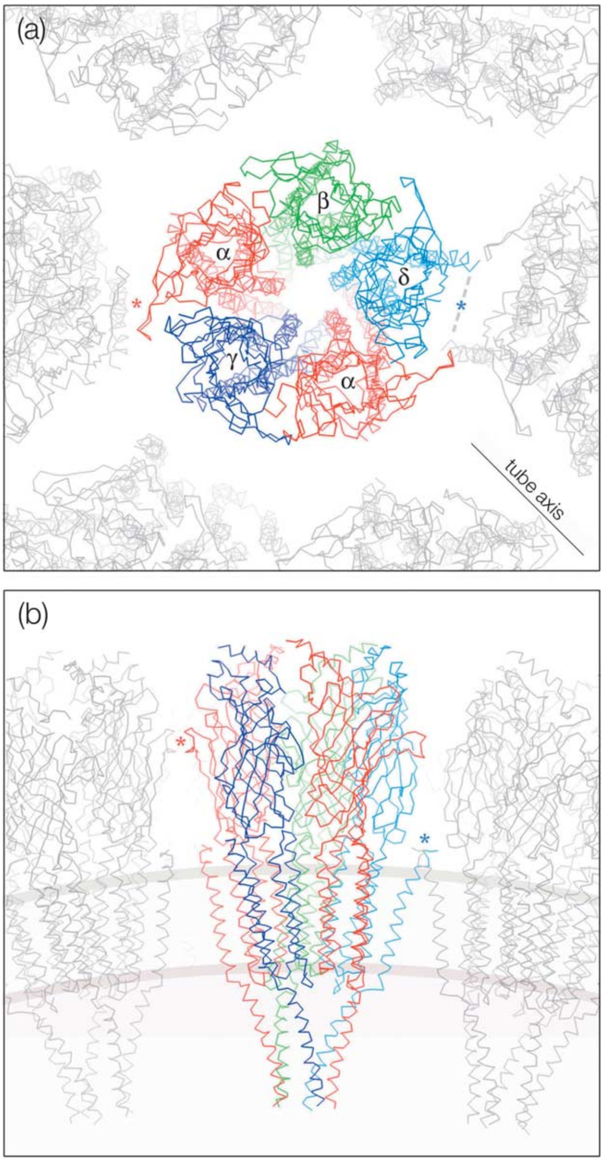

Figure 1. Packing of receptors in the p2 tubular surface lattice. (a) View down the axis of a single receptor and (b) view from the side, parallel with the membrane plane. Individual receptors are embedded in a curved lipid matrix and come closest to each other at radial 2-fold axes (asterisks in (a)). A disulphide bridge between cysteine residues of neighbouring δ subunits lies at one such axis (blue asterisk); the C loops of neighbouring α subunits (α$_γ$) lie at the other (red asterisk). The direction of the tube axis and location of the membrane are indicated in (a) and (b), respectively. The cysteine residues at the 2-fold axis are the penultimate residues of the δ subunits (see Figure 5), and are in a region of weak densities where the polypeptide chain could not be traced (broken line in (a)). Individual subunits are in different colours (α, red; β, green; γ, blue; δ, light blue).

several interactions at the subunit interfaces, and within the α subunits, which may be responsible for their "distorted" structures. The ACh-binding site itself, which was not correctly identified in the 9 Å map,[13] shows many features that are apparent in the structure of AChBP. However, the organisation of the B and C loops at the binding site of the closed channel differs from that in AChBP, where ligand is present, indicating that the binding reaction is accompanied by a local structural rearrangement. A comparison of the two structures suggests how the local rearrangement associated with ACh binding stabilises the alternative open-channel form of the receptor. Given our improved understanding of this initial step, it is now possible to sketch a complete picture of the series of coordinated events leading to opening of the channel. Finally, we discuss the role of the vestibules, the ionic surfaces of which create a strongly electronegative environment at either entrance of the narrow membrane pore.

Results

Structure refinement

The original 4 Å data set was from 359 images of tubes,[10] grown from *Torpedo marmorata* postsynaptic membranes.[15] The tubes have four distinct helical symmetries, with individual molecules arranged on a p2 surface lattice[15] such that the inside of the tube corresponds to the inside of the cell.[29] The receptors come closest to each other near radial 2-fold axes (Figure 1(a)). A disulphide bridge between the δ subunits of neighbouring receptors[30,31] lies near the membrane at one such axis; the α-subunit C loops of neighbouring receptors lie ∼40 Å from the membrane at the other (Figure 1(b)). We chose to refine the receptor structure using standard crystallographic methods, by neglecting these minimal interactions and placing the experimental densities corresponding to a single molecule into an artificial unit cell (see Methods). To validate this approach, we monitored the agreement between the phases along layer-lines obtained by Fourier transformation of the images and the equivalent phases calculated from model tubes. The helical phase residual, comparing the experimental and calculated terms, provided an independent objective measure of the accuracy of the structure.

A starting model of the receptor was built from the coordinates of partial structures determined in earlier studies and from α-helical segments fitted to the densities shaping the intracellular vestibule (see Methods). Starting sets of phases were also calculated from these coordinates after incorporating them into models of each of the four kinds of tube. More detailed coordinates were substituted later. While at first the coordinates and hence the models were incomplete and only approximate, reductions in the crystallographic *R*-factors, paralleled by lower helical phase residuals, showed that the models became more accurate as the refinement proceeded.

As a preliminary step in the refinement, we used the phases calculated from the model tube structures as a reference to assess and optimise the quality of the original data set. The model-derived phases provided a more sensitive test of the signal retained in the images at high resolution than the previous reference, which had been derived solely from the images. In this way, we found that elimination from each helical family of a fraction of the layer-lines, the amplitudes along which were dominated by noise (see Methods), improved the quality of the data significantly (Table 1). Elimination of 17 "bad" images, for which the Fourier phases showed no significant correlation with calculated values at resolutions better than 11 Å also brought about some improvement (Table 1). It appeared that these images contributed disproportionately large amplitude errors as a result of overlap of terms along the layer-lines (see Methods).

The refinement of the structure was performed by first treating the inner and outer β-sheet fragments, the membrane-spanning portion and the intracellular α-helices of each subunit as separate rigid units. A major drop in R_{free} and in the helical phase residuals (Table 1) was achieved by reducing the *a* and *b* unit cell dimensions (lying parallel with the membrane plane). The values of these parameters and the positional alignments were carefully optimised by several cycles of rigid-body refinement, minimising R_{free}. The decrease in the *a* and *b* unit

Table 1. Comparison between experimental and calculated phases along layer-lines during refinement

Helical family				Steps
(−16,6)	(−17,5)	(−15,7)	(−18,6)	
62.19	66.17	67.86	64.06	(1)
59.99	62.52	63.94	60.57	(2)
58.79	62.02	63.72	60.15	(3)
53.96	54.36	59.86	55.94	(4)
53.57	54.61	57.92	56.16	(5)

Amplitude-weighted phase differences; resolution range, 100–4 Å; number of Fourier terms used for each estimate, $\sim 1.1\times 10^5$. (1) Initial model: inner and outer sheets of ligand-binding domain, membrane-spanning domain, intracellular MA helices. (2) Elimination of noisy layer-lines from original data (see Methods). (3) Elimination of bad images (17 out of 359). (4) Rigid-body refinement of fragments and domains; refinement of unit cell. (5) Molecular dynamics energy minimisation; modelling of loop regions; manual adjustments of side-chains.

Table 2. Refinement statistics

P1 unit cell (refined) (Å)	$a=129.6$, $b=129.6$, $c=174.5$
Resolution range (Å)	100–4
R_{cryst} (%)	36.7
R_{free} (%)	37.9
Fourier terms	95,988
rms deviations	
Bond lengths (Å)	0.016
Bond angles (deg.)	2.16
Average B-factor (Å^2)	67.2
Ramachandran analysis (%)	
Most favoured	77.1
Allowed	19.5
Generously allowed	3.4
Disallowed	0.0

cell dimensions as a result of the optimisation was 2.6%, implying that the averaged structure composing the tubes was at a smaller radius than it appeared in the images. A minor degree of flattening probably contributed this effect, since departure from a circular cross-section would cause the Fourier amplitudes to fall off more rapidly in the radial direction, a result suggested by the values obtained for the overall anisotropic temperature factors ($B_{11}=-21.3$ Å^2; $B_{22}=-21.3$ Å^2; and $B_{33}=42.6$ Å^2, where B_{33} refers to this direction).

Additional improvements were obtained by several cycles of molecular dynamics refinement, using energy minimisation and backbone hydrogen-bond restraints, followed by manual rebuilding and extension of loop regions, in O.[32] The final R-factors were: $R_{\mathrm{cryst}}=36.7\%$; $R_{\mathrm{free}}=37.9\%$ (Table 2). At these values the phase residuals had reached their minimum values, implying that the best accuracy of structure, limited by the resolution and by the amplitudes determined from images, had been achieved. The quality of the density map had enabled placement of 80% of the 2335 amino acid residues, the missing residues being located mostly in the M3–M4 intracellular loop, but also in the β7–β8 loops of the non-α subunits, and the C termini (12 and 17 residues) of the γ and δ subunits. However, several of the loop regions were poorly defined compared with the rest of the structure, making the tracing in these regions less reliable and precluding detailed interpretation. The refinement

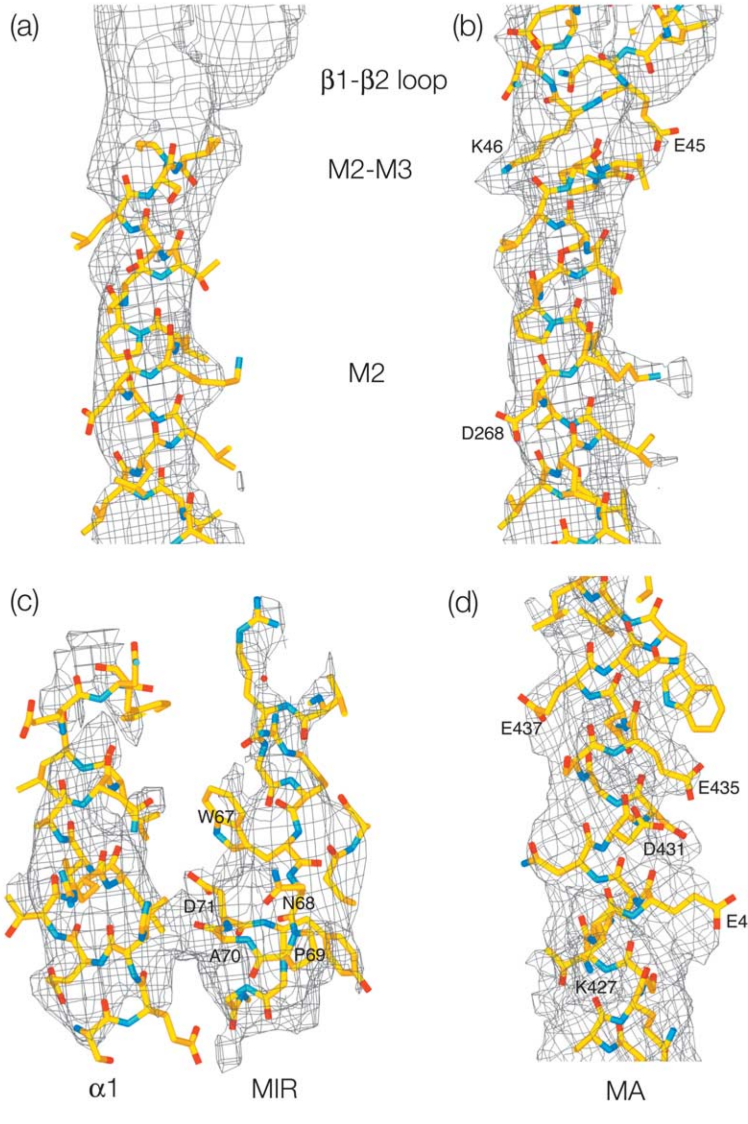

Figure 2. Examples of polypeptide chains superimposed over the densities in different regions of the experimental density map. (a) This is a view of the "upper" part of the helix M2 (β subunit) in the original map (PDB entry 1OED), and (b) is the same region (including the β1–β2 loop) after refinement and improvement of the density map (see Methods); the residues K46 and E45 of the β1–β2 loop lie over the M2–M3 linker, and D268 is a component of the extracellular ring of negative charge.[21] (c) The main immunogenic region (MIR) of the α subunit next to δ (α_δ) and the adjacent N-terminal α-helix, as viewed from the synaptic cleft; the labelled residues W67–D71 contribute most to the antigenicity of the MIR (see Figure 5). (d) The helix MA (γ subunit), shaping the intracellular vestibule of the channel, as viewed from the adjacent α_γ subunit; charged residues are labelled (see also Figures 7 and 8(b)). Contours are at 2σ.

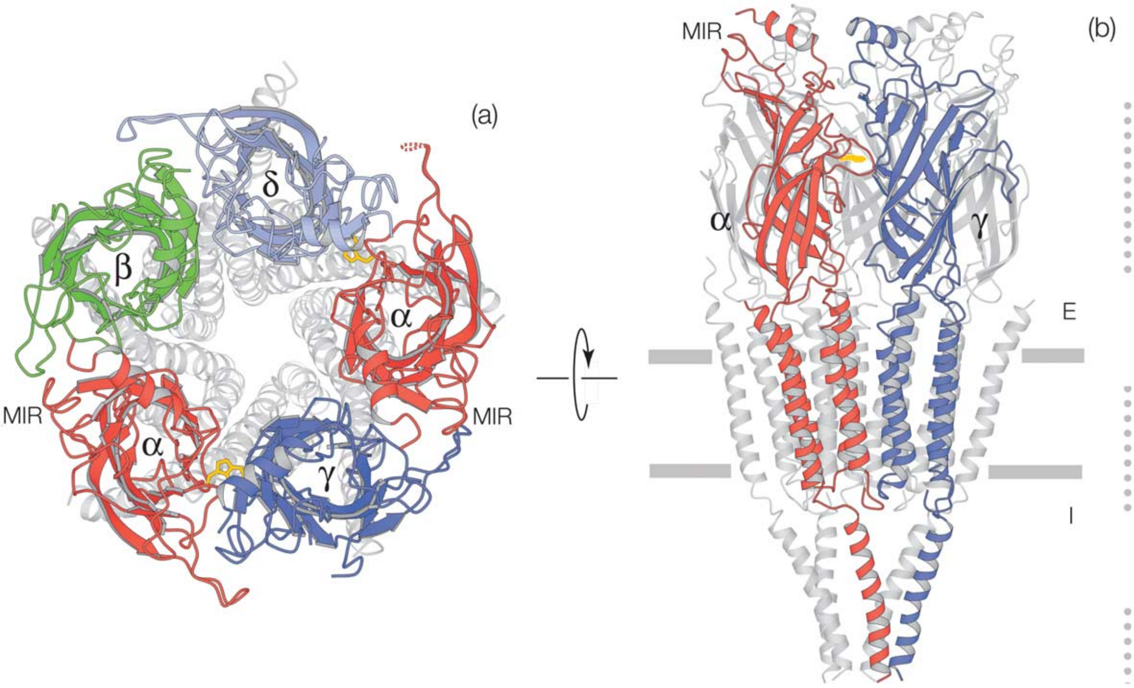

Figure 3. Ribbon diagrams of the whole receptor, as viewed (a) from the synaptic cleft and (b) parallel with the membrane plane. For clarity, only the ligand-binding domain is highlighted in (a) and only the front two subunits are highlighted in (b) (α, red; β, green; γ, blue; δ, light blue). Also shown are the locations of αTrp149 (gold), the MIR and the membrane (horizontal bars; E, extracellular; I, intracellular). The dotted lines on the right denote the three main zones of subunit–subunit contacts. The apex of the C-loop of α_δ (broken trace in (a)) was not visible in the densities.

led to relatively modest changes in membrane-spanning structure ($\text{rmsd}_{C\alpha}=0.8$ Å) compared with the original model.[10] The final refined model showed no residues (except for Gly) having dihedral angles in the disallowed region of the Ramachandran plot.

Three-dimensional density map

Examples of the polypeptide chains superimposed on the experimental densities are given in Figure 2. Figure 2(a) and (b) compare details of a membrane-spanning helical segment (M2 of the β subunit) in (a) the original model, and (b) after the refinement. As is typical of the membrane-spanning region, the positions of most of the side-chains have not changed much as a result of the refinement; on the other hand, the densities have improved, giving better definition for the bulky hydrophobic and extended side-chains. Thus we now have greater confidence that the assignments made in the original study were correct, even if at the present resolution the conformations of individual side-chains cannot be determined.

In a density map from a helical structure, the signal-to-noise ratio may vary, depending on distance from the helix axis: at high radius, high-order Bessel terms are mainly responsible for the density variations, and the retention of these terms depends on the accuracy of distortion corrections;[33] at low radius, the spatial overlap of different Bessel orders, which increases with resolution, becomes a potential source of additional noise.[14] However, we now find that the large side-chains are defined with roughly equal clarity at either end of the structure (Figure 2(c) and (d)), making it unlikely that these effects have seriously compromised the overall quality of the map.

Architecture and fold

The receptor is composed of elongated subunits, which associate with their long axes approximately normal to the membrane, creating a continuous wall around the central ion-conducting path. The whole assembly presents a rounded, nearly 5-fold symmetric shape when viewed from the synaptic cleft (Figure 3(a)), but is wedge-shaped when viewed parallel with the membrane plane (Figure 3(b)).

The subunits of the receptor all have a similar size (maximum dimensions 30 Å×40 Å×160 Å) and the same three-dimensional fold. Figure 4 illustrates this fold, as viewed in face-on and side-on orientations relative to the axis of the channel. Each subunit is a three-domain protein and so partitions the channel naturally into its ligand-binding, membrane-spanning and intracellular parts. The N-terminal, extracellular portion is built around a β-sandwich core consisting of ten β-strands (inner sheets, blue; outer sheets, red) and contains one α-helix, like the protomer of AChBP.[6] This portion also contains several loop regions (e.g. the loops A, B and C, the Cys loop and

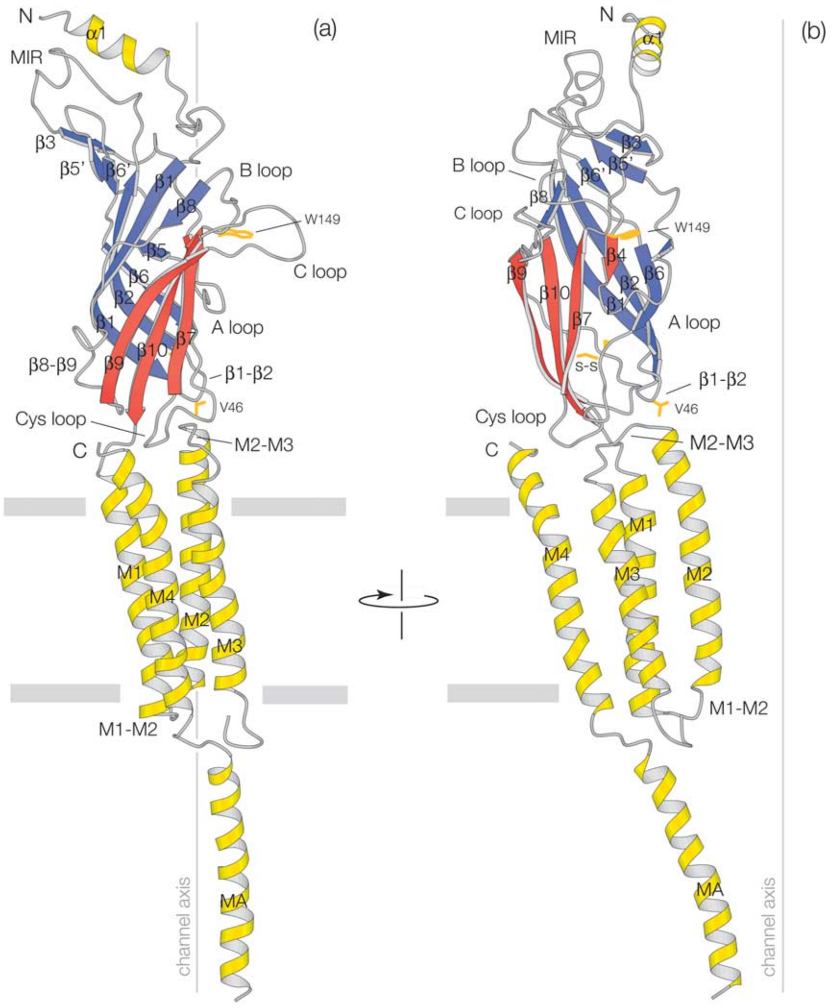

Figure 4. Ribbon diagrams of a single subunit (α) viewed parallel with the membrane plane, in orientations such that the central axis of the pentamer (vertical line) is (a) at the back and (b) to the side. The α-helices are in yellow; the β-strands composing the β-sandwich are in blue (inner) and red (outer). Locations of the N and C termini, αTrp149, αV46, the Cys-loop disulphide bridge and the membrane (horizontal bars) are indicated. Part of the M3–M4 loop (connecting MA to M3) is missing. Labelling of secondary structural elements and loops in this Figure and Figure 5 corresponds to that given in previous publications.[6,10,34]

the β1–β2 loop), which are critical for receptor function. The membrane-spanning portion is composed of four α-helical segments, M1–M4, and the functionally important M1–M2 and M2–M3 loops. It is joined covalently to the extracellular domain at the end of M1, and also interacts, through M2–M3, with the β1–β2 and Cys loops. The intracellular portion is composed mainly of the stretch of sequence between M3 and M4, and includes a curved α-helix, MA,[34] which precedes M4. Most of the rest of M3–M4 (i.e. M3–MA) appears to be disordered and is not seen in the structure.

Figure 5 shows how the structural elements of the α polypeptide chain are organised in relation to the amino acid sequence. The aligned β, γ and δ chains have the same organisation, and their corresponding three-dimensional structures closely resemble that of the α chain, except in some short non-conserved regions (e.g. in the β8–β9 and C loops).

Symmetry

The approximate 5-fold symmetry of the receptor was examined further by determining the angles required to achieve optimal least-squares superposition of the subunits around the pentamer. Deviations from 5-fold were found to be smallest in the membrane-spanning domain, where each subunit assumed an orientation lying within 2° (s.d. = 1.61°) of the value required for exact register with a 5-fold-averaged structure. These deviations appeared to be a consequence of structural variations (which are most pronounced with M4[10]) arising from the non-identical amino acid sequences. However, the deviations from 5-fold were greater in the ligand-binding domain, because the two α subunits achieved exact register at rotation angles quite different from those of the other three. Using superpositions of the 190 most closely matched C^α atoms, for example, the deviations were: $\alpha_\gamma = -3.17°$; $\beta = +0.85°$; $\gamma = +2.71°$; $\delta = +3.71°$; $\alpha_\delta = -4.08°$ (α_γ is the α subunit next to γ; minus is anticlockwise, viewed from the synaptic cleft). Hence there is an apparent anticlockwise rotation of the α subunits relative to the non-α subunits in the ligand-binding domain. This apparent rotation reflects the fact that the α subunits in the closed channel have a distinct

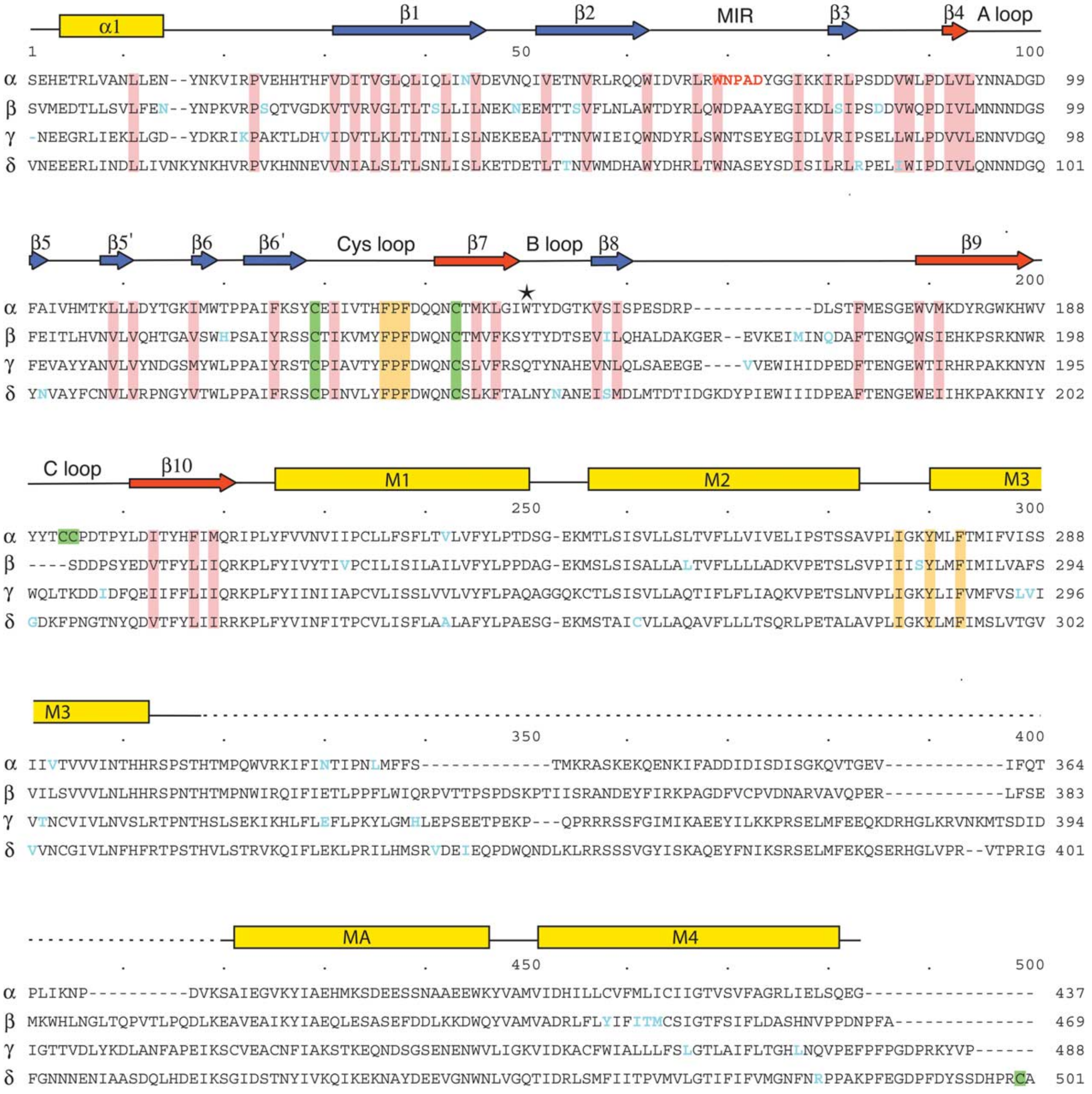

```
1         .         .         .         .         50        .         .         .         .         100
α SEHETRLVANLLEN--YNKVIRPVEHHTHFVDITVGLQLIQLINVDEVNQIVETNVRLRQQWIDVRLRWNPADYGGIKKIRLPSDDVWLPDLVLYNNADGD  99
β SVMEDTLLSVLFEN--YNPKVRPSQTVGDKVTVRVGLTLTSLLILNEKNEEMTTSVFLNLAWTDYRLQWDPAAYEGIKDLSIPSDDVWQPDIVLMNNNDGS  99
γ -NEEGRLIEKLLGD--YDKRIKPAKTLDHVIDVTLKLTLTNLISLNEKEEALTTNVWIEIQWNDYRLSWNTSEYEGIDLVRIPSELLWLPDVVLENNVDGQ  98
δ VNEEERLINDLLIVNKYNKHVRPVKHNNEVVNIALSLTLSNLISLKETDETLTTNVWMDHAWYDHRLTWNASEYSDISILRLRPELIWIPDIVLQNNNDGQ 101

          .         .         .         .         .         .         .         .         200
α FAIVHMTKLLLDYTGKIMWTPPAIFKSYCEIIVTHFPFDQQNCTMKLGIWTYDGTKVSISPESDRP------------DLSTFMESGEWVMKDYRGWKHWV 188
β FEITLHVNVLVQHTGAVSWHPSAIYRSSCTIKVMYFPFDWQNCTMVFKSYTYDTSEVILQHALDAKGER--EVKEIMINQDAFTENGQWSIEHKPSRKNWR 198
γ FEVAYYANVLVYNDGSMYWLPPAIYRSTCPIAVTYFPFDWQNCSLVFRSQTYNAHEVNLQLSAEEGE----VVEWIHIDPEDFTENGEWTIRHRPAKKNYN 195
δ YNVAYFCNVLVRPNGYVTWLPPAIFRSSCPINVLYFPFDWQNCSLKFTALNYNANEISMDLMTDTIDGKDYPIEWIIIDPEAFTENGEWEIIHKPAKKNIY 202

          .         .         .         .         250       .         .         .         .         300
α YYTCCPDTPYLDITYHFIMQRIPLYFVVNVIIPCLLFSFLTVLVFYLPTDSG-EKMTLSISVLLSLTVFLLVIVELIPSTSSAVPLIGKYMLFTMIFVISS 288
β ----SDDPSYEDVTFYLIIQRKPLFYIVYTIVPCILISILAILVFYLPPDAG-EKMSLSISALLALTVFLLLLADKVPETSLSVPIIISYLMFIMILVAFS 294
γ WQLTKDDIDFQEIIFFLIIQRKPLFYIINIIAPCVLISSLVVLVYFLPAQAGGQKCTLSISVLLAQTIFLFLIAQKVPETSLNVPLIGKYLIFVMFVSLVI 296
δ GDKFPNGTNYQDVTFYLIIRRKPLFYVINFITPCVLISFLAALAFYLPAESG-EKMSTAICVLLAQAVFLLLTSQRLPETALAVPLIGKYLMFIMSLVTGV 302

          .         .         .         .         350       .         .         .         .         400
α IIVTVVVINTHHRSPSTHTMPQWVRKIFINTIPNLMFFS-------------TMKRASKEKQENKIFADDIDISDISGKQVTGEV------------IFQT 364
β VILSVVVLNLHHRSPNTHTMPNWIRQIFIETLPPFLWIQRPVTTPSPDSKPTIISRANDEYFIRKPAGDFVCPVDNARVAVQPER------------LFSE 383
γ VTNCVIVLNVSLRTPNTHSLSEKIKHLFLEFLPKYLGMHLEPSEETPEKP---QPRRRSSFGIMIKAEEYILKKPRSELMFEEQKDRHGLKRVNKMTSDID 394
δ VVNCGIVLNFHFRTPSTHVLSTRVKQIFLEKLPRILHMSRVDEIEQPDWQNDLKLRRSSSVGYISKAQEYFNIKSRSELMFEKQSERHGLVPR--VTPRIG 401

          .         .         .         .         450       .         .         .         .         500
α PLIKNP----------DVKSAIEGVKYIAEHMKSDEESSNAAEEWKYVAMVIDHILLCVFMLICIIGTVSVFAGRLIELSQEG-----------------  437
β MKWHLNGLTQPVTLPQDLKEAVEAIKYIAEQLESASEFDDLKKDWQYVAMVADRLFLYIFITMCSIGTFSIFLDASHNVPPDNPFA--------------  469
γ IGTTVDLYKDLANFAPEIKSCVEACNFIAKSTKEQNDSGSENENWVLIGKVIDKACFWIALLLFSLGTLAIFLTGHLNQVPEFPFPGDPRKYVP------  488
δ FGNNNENIAASDQLHDEIKSGIDSTNYIVKQIKEKNAYDEEVGNWNLVGQTIDRLSMFIITPVMVLGTIFIFVMGNFNRPPAKPFEGDPFDYSSDHPRCA  501
```

Figure 5. Aligned amino acid sequences of the four ACh receptor polypeptide chains. The sequences are from *T. marmorata*, which differ in 48 places (cyan lettering) from those of *T. californica* (including the absence of the first residue of γ). Locations of the MIR (critical segment in red), named loops, αTrp149 (star), and some key cysteine residues (green background) are indicated. Conserved residues forming the hydrophobic cores of the subunits in the ligand-binding domain and at the boundary between this domain and the membrane-spanning domain are shown with pink and orange background, respectively. Elements of secondary structure, for the α subunits, are indicated above the sequences (yellow, α-helix; blue and red, β-strands composing the inner and outer sheets of the β-sandwich). The exact extents of the α-helices and β-strands are not accurately represented, given the limited resolution, but are similar for all four polypeptides.

conformation,[17] associated with an alternative arrangement of the β-sheets.[18] The different subunit conformations will be described in detail later.

Subunit–subunit interfaces

The main contacts between neighbouring subunits occur at three levels in the structure (dotted lines, Figure 3(b)), and each of the interfaces exhibits similarly extensive subunit–subunit interactions. Figure 6 tabulates the tentative interactions made between the α subunits and the adjacent β, γ and δ subunits, based on the estimates of side-chain positions in the refined structure and assuming a cut-off distance for interacting atoms of 3.9 Å. We call the binding-site/disulphide-bridge side of the subunit, the + side; and the other side, the − side. On the + side, residues of the B loop and inner sheet, M2, M3, M3–MA and MA interact with residues of the inner sheet, M2, M1, M1–M2 and

β	γ	α		γ	δ
+		−	+	−	
A, B, C loops		*inner sheet*	*B loop, inner sheet*	*inner sheet*	
E155 Y151 T150 Y149	**E154** Y150 N151 T149 Q98 T199 **D96** **E46**	**R79** **K107** T106 I102 P121 I38 I41 N42	**K155** Y151 **D152** T150 W149 Y127	I74 L76 **R78** N106 L118 P119 P120 N38	L80 **R81** **R83** N109 P122 P123
M2		*M2*	*M2*	*M2*	
D268 L264 V261 T260 L257 I253 S250	F266 I263 T262 L259 I255	L263 F256 S252 V249 S248 L245	**E262** L258 V255 T254 L251 I247 T244 M243	**K271** F264 I263 A260 S256	**R277** F270 A266 V263 C262 T259
M3		*M1*	*M3*	*M1*	
N303 H306	V301 L304 L308	F227 L231 Y234 L235 **D238**	I289 V293 N297 H300	L231 S234 L242	L238 F241 L245
M3-MA		*M1-M2*	*M3-MA*	*M1-M2*	
P309 T311 H312	**R309** H314 T310	**K242** S239 **E241**	**R301** H306 S302 P303 S304	**K250** Q245 Q249 G247	**E252** S253
MA		*MA*	*MA*	*MA*	
I411 I408 A404	I422 C419 V416 C415	**E384** **K380** **E377**	M386 A383 I382 V379 I376	**K427** **K424** N420	**K434** **K431** I423

Figure 6. Closely apposed residues at the interfaces of the α subunits with neighbouring β, γ and δ subunits. The + symbol denotes the interface on the binding-site/disulphide-bridge side of the subunit (i.e. on the right face, Figure 4a); the − symbol denotes the interface on the distant side (left face, Figure 4(a)). Residues in each column are grouped according to their level in the structure (C^{α} positions, beginning from the extracellular end) and categorised according to the structural elements harbouring them. Charged residues are in bold font.

MA of the γ and δ subunits. On the − side, residues of the inner sheet, M2, M1, M1–M2 and MA interact with residues of the A, B and C loops, M2, M3, M3–MA and MA of the β and γ subunits.

The subunits in the ligand-binding domain interact mainly through polar side-chains. Similar sets of interactions occur in AChBP,[6] but they are more extensive in the latter, consistent with the fact that AChBP (in the presence of ligand) has a smaller radius of gyration (29.8 Å compared with 31.8 Å for the ligand-binding domain, calculated from the atomic coordinates), and so is more compact. It is notable that the interfaces on both sides of the α subunits contain charged side-chains, which form probable ion pairs with side-chains on neighbouring subunits (αR79 with βD155, γE154; αD152 with γR78, δR81). These interactions may be important in stabilising the resting, closed-channel conformation of the α subunits. There are no equivalent pairings between charged side-chains at the non-α, β–δ interface.

In the domain shaping the membrane pore, hydrophobic side-chains projecting from the helices M1, M2 and M3 are mainly responsible for the subunit–subunit contacts. A probable exception is an interaction involving positively charged side-chains on δ, γ (R277, K271) with the side-chains E262 of the α subunits composing the pore-lining "extracellular ring".[21] The subunit–subunit contacts between the helices occur predominantly in the intracellular leaflet of the bilayer, and implicate relatively few residues on M1 and M3 (Figure 6). At the intracellular face of the membrane-spanning domain, and at the extreme intracellular end of the receptor, there are several additional subunit–subunit contacts implicating the M1–M2 loop, the M3–MA loop and MA. However, the description of these regions may be incomplete, given that parts of the M3–MA loop may be involved that are not visible in the structure.

The narrow interstitial spaces between the contact areas on the subunit interfaces are of special interest because they provide pathways (or potential pathways) for diffusing ions. Most of them are lined by polar or negatively charged side-chains and would therefore be selectively permeable to cations. They occur on both sides of the membrane close to the membrane surfaces. However, the largest open spaces are on the intracellular side, between neighbouring MA helices, and the surfaces framing each of these contain several negative charges (Figure 7).

The intracellular MA helices from each subunit together create an inverted pentagonal cone having five intervening open spaces, or windows, of similar size. These windows represent obligatory ion pathways, since no alternative routes exist for transport into, or out of the intracellular vestibule. The windows have a maximum width of only ∼8 Å, which is comparable with the diameter of a sodium or potassium ion surrounded by its first hydration shell. The windows would therefore force direct interaction of the hydrated ion with their negatively charged surfaces, facilitating cation transport while electrostatically repelling anions and preventing large ions from going through.

The vestibules

The extracellular and the intracellular vestibules are both narrow enough (∼20 Å wide) to ensure that charged groups lining their surfaces would interact electrostatically with the passing ions, yet wide enough not to necessitate direct contact, which could slow their movement.[11] Again, the charged groups are almost entirely of negative polarity (Figure 8(a) and (b)). The resulting cation-stabilising environments would increase the concentration of cations relative to that of anions at both entrances of the narrow membrane pore, and so promote

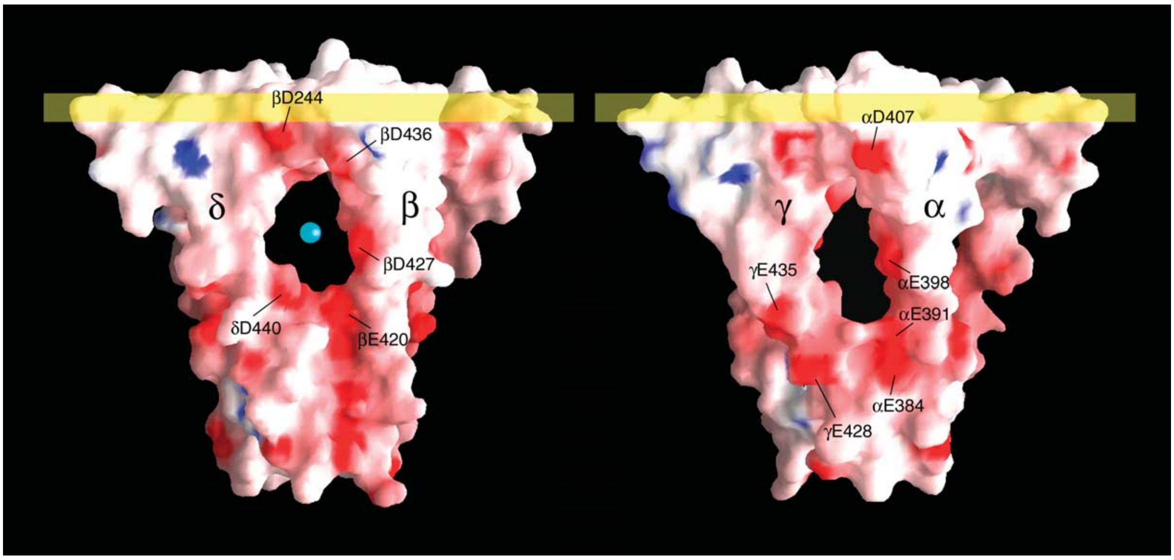

Figure 7. Electrostatic potential surface representations showing entry/exit windows for cations between the MA helices of different subunits on the intracellular side of the membrane. The windows formed between δ and β, and between γ and α_δ, are on the left and right, respectively. Labels identify exposed charged side-chains. The location of the intracellular membrane surface is indicated (horizontal bars). The sphere in the δ–β window is the size of a potassium ion (2.7 Å diameter). Portions of the polypeptide chain other than MA are involved in shaping the upper portions of the windows; the stretches in the Figure, and in Figure 8(b), are from: α233–α248 (including the M1–M2 loop); α295–α306 (including the C terminus of M3); α374–α411 (including the N terminus of M4). The electrostatic surface was contoured between $-15kT/\mathrm{e}$ and $+15kT/\mathrm{e}$; negative and positive charge in red and blue, respectively.

efficient bidirectional transport of cations through the open channel. As will be discussed later, it is likely that the vestibules (including the intracellular windows) contribute significantly to the charge selectivity of the channel, and that the "selectivity filter" is not just a local region, identified by mutation experiments, at the intracellular end of the pore.

Interactions across subunit domains

Several components of the ligand-binding domain could in principle be involved in communicating the ACh-triggered conformational change to the membrane-spanning domain, where the gate is located. But the structure (Figure 4) shows that only the Cys loop, the β1–β2 loop and the polypeptide chain (through the covalent connection) make direct contact. The two loops interact with the stretch of amino acid residues M2–M3, linking the M2 and M3 helical segments: the Cys loop by straddling M2–M3 near the N terminus of M3, and the β1–β2 loop by straddling M2–M3 near the C terminus of M2. It is notable that the Cys and β1–β2 loops are not in equivalent locations relative to the membrane-spanning domain for all subunits around the pentamer (Figure 9(a)). In the α subunits (which have a special conformation; see below) they are slightly displaced along M2–M3, bringing the β1–β2 loop 2–3Å closer to the axis of the channel.

The interaction of these loops with M2–M3 involves different amino acid residues, depending on the subunit in question and, in the case of the Cys loop, implicates additional residues near the ends of M1 and M4. However, one set of interactions, involving the consecutive residues FPF, of the Cys loop, and the residues I, Y and F (aligning with αI274, αY277 and αF280) at the end of M3, is common to all five subunits. The FPF residues project downward from the extremity of the Cys loop towards the membrane to meet the I, Y and F residues extending upward from M3 towards the ligand-binding domain (Figure 9(b)). These six residues are highlighted in Figure 5 (orange background): together they form a cluster, the hydrophobic and predominantly aromatic character of which is conserved throughout the receptor superfamily. The flexible aromatic residues may serve to accommodate movements that occur near the end of M3 during gating (see below), as well as to anchor the Cys loop to the membrane-spanning domain.

Two residues of the β1–β2 loop appear to be important in forming interactions with M2–M3: the residue aligning with αV46 and the adjacent glutamic acid residue (aligning with αE45), which is conserved throughout the superfamily. Their side-chains together make an arc embracing the M2–M3 backbone, and may therefore help to fix the end of M2, which is not in contact with the other membrane-spanning helices at this level in the structure. The αV46 side-chain (V44 in AChBP) fits into a hydrophobic pocket made by the end residues of M2,[10] consolidating the clasp. However, the side-chains equivalent to αV46 in the other subunits seem slightly displaced from the ends of the M2 helices (Figure 9(a)) and do not make equivalent contacts: for example, the lysine residue

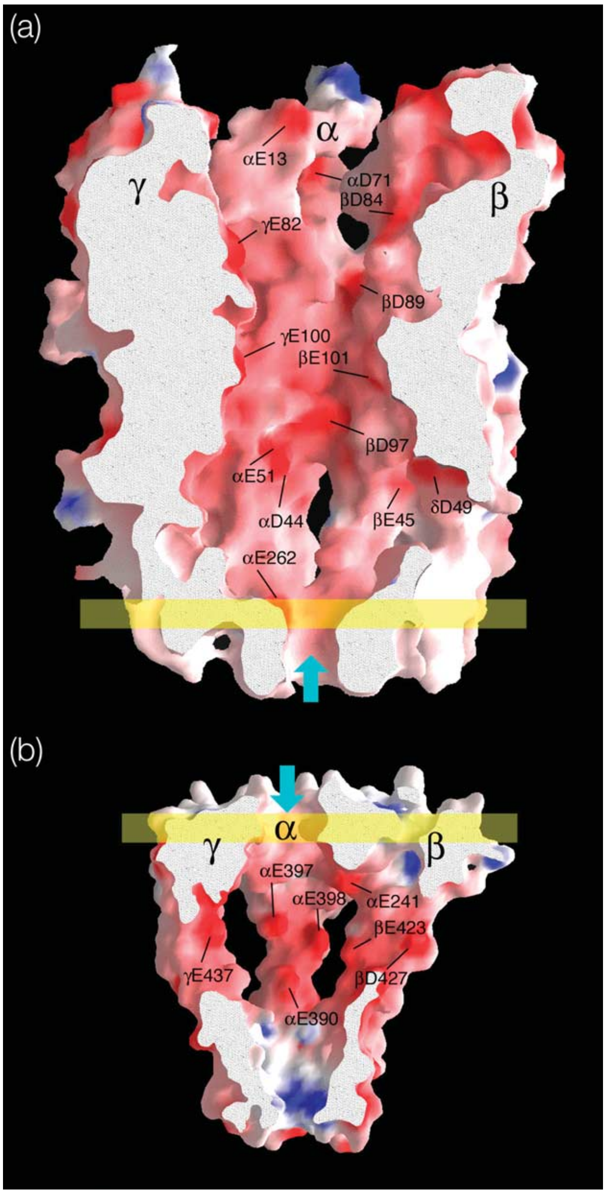

Figure 8. Central sections showing the inner surfaces of (a) the extracellular and (b) the intracellular vestibules. Both vestibules are lined by an excess of negatively charged groups, promoting a cation-stabilising electrostatic environment. (a) A view looking towards the α_{γ}–β subunit–subunit interface; (b) a view looking towards the α_{γ} subunit, with γ and β on either side. Labels identify exposed charged side-chains. The locations of the membrane pore (arrows) and the membrane surfaces (horizontal bars) are indicated. Electrostatic surfaces are contoured as in Figure 7.

on the β subunit (βK46) overlies M2–M3, with the terminal amino group apparently exposed to solvent (Figure 2(b)).

Conformations of individual subunits

The conformations of the subunits in the closed channel were investigated in an earlier study[18] by dividing the β-sandwich core of the AChBP protomer into the inner and outer β-sheet fragments, and fitting these fragments as rigid bodies to a 4.6 Å resolution density map. This study had suggested that to a first approximation there are two alternative arrangements of the sheets related by rotations about the Cys-loop disulphide bridge: one arrangement characteristic of the two α subunits and the other characteristic of the three non-α subunits. However, the relatively poor quality of the 4.6 Å map, omission of loop regions and the strict rigid-body approach limited the conclusions drawn. The refined, energy-minimised structure, described here, allowed a more accurate assessment of the alternative conformations of the subunits.

To conduct an initial comparison, we rotated each subunit by a multiple of 72° about an axis normal to the membrane plane to bring it into 5-fold register with a reference subunit. We then aligned it translationally to superimpose the midpoints of the lines connecting the C^{α} atoms of the pair of cysteine residues forming the disulphide bridge. This comparison confirmed that the inner sheets of both α subunits were rotated anticlockwise relative to those of the other subunits, when viewed from the synaptic cleft (curved arrow, Figure 10(a)). The individual C^{α} traces showed systematic differences, distinct from differences which could arise from similar, but non-identical subunit structures or from inaccuracies in chain tracing. As before, the rotation axis of the inner sheets was normal to the membrane and in the vicinity of the disulphide bridge. However, to achieve pairwise least-squares superpositions of the inner sheets onto α_{γ}, the angles were: $\alpha_{\delta}=+1.6°$; $\beta=+10.9°$; $\gamma=+11.2°$; $\delta=+11.7°$. That is, the measured rotation angles of the α chains, relative to the non-α chains, were about 5° smaller than the values (~15°) estimated previously.

While the anticlockwise rotations in the α subunits applied to the entire set of inner β-strands, including the loop (β2–β3) harbouring the main immunogenic region (MIR), the adjacent N-terminal α-helices were not significantly rotated, but retained orientations similar to those of the non-α subunits. As a result, the α subunits have the N-terminal helix and the MIR separated by a cleft (Figure 2(c)). The wider separation between these two regions in the α subunits may reflect small differences compared with the non-α subunits in the set of interactions that hold the N-terminal helix in place. This helix is not tightly associated with the body of the subunit as it is in AChBP.

We also confirmed the previous finding that the strands composing the outer sheet of the β-sandwich tilt more steeply in the case of the α than the non-α subunits, when viewed from a direction parallel with the membrane plane (Figure 10(b)). However, the differences in tilt of the individual strands (β9, β10, β7 and β4) was not uniform, since the strand β9 of the α subunits runs almost parallel with those of the non-α subunits, and the strand β10 is intermediate between the two

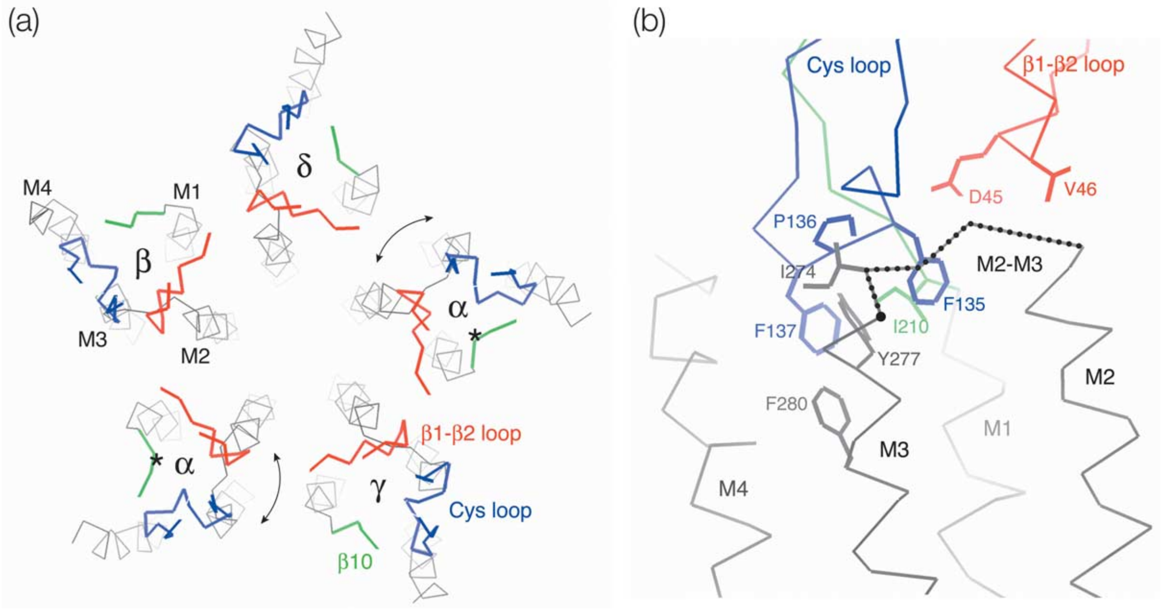

Figure 9. Interaction of loops at the boundary between the ligand-binding and membrane-spanning domains. (a) This is a view down the central axis of the receptor showing, for each subunit, the locations of the Cys loop (α128–α142) and the β1–β2 loop (extended to include α41–α50) in relation to the underlying domain forming the membrane pore; the asterisk and arc on both α subunits indicates the position of the rotation axis relating the inner sheets (see Figure 11(a)). (b) This is a view of the domain boundary (α subunit) from the side, showing the Cys loop and β1–β2 loop in relation to M2–M3 (dotted trace), and the locations of residues mentioned in the text; the large dot at the M3 end of the M2–M3 trace denotes a conserved glycine residue (αG275), which may provide a point of flexure during gating. The Cys loop, the β1–β2 loop, the extension of M1 into strand β10 of the ligand-binding domain, and components of the membrane-spanning domain are in blue, red, green and grey, respectively.

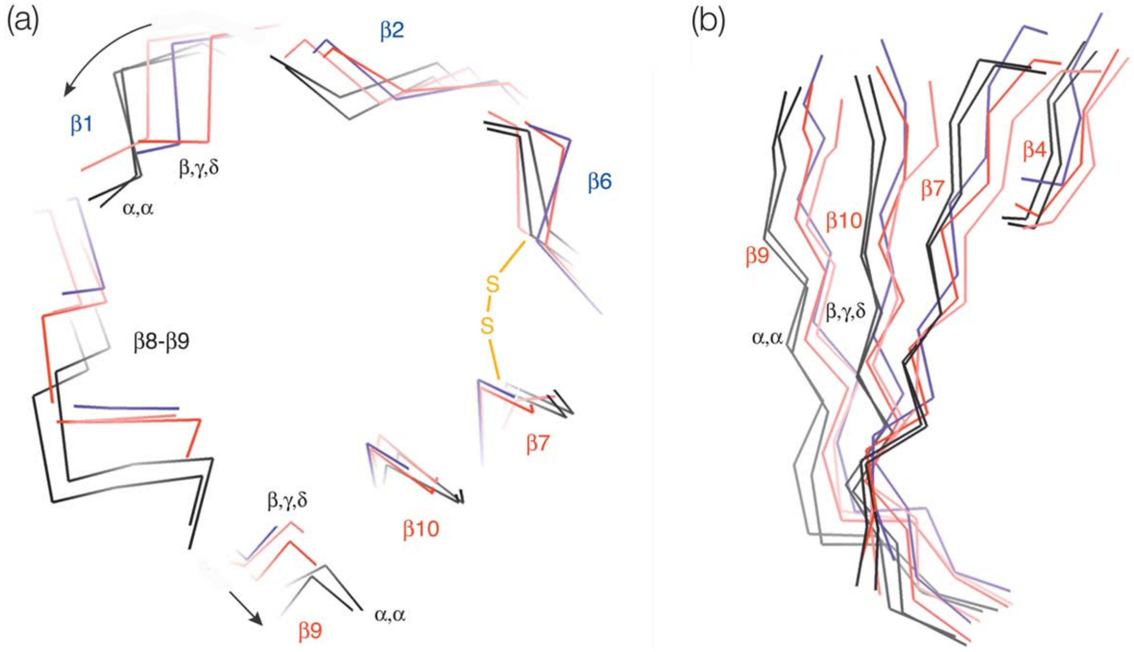

Figure 10. Superposition of backbone C^{α} traces of portions of the subunits after they have been rotated by multiples of 72° to bring them into 5-fold register and aligned on the Cys-loop disulphide bridge. The slabs shown lie (a) parallel with and (b) obliquely to the membrane plane. (a) A cross-section through the subunits at the level of the disulphide bridge (S–S), as viewed from the synaptic cleft; the curved arrow denotes the anticlockwise rotation of the inner β-strands of the α subunits, relative to those of the non-α subunits; the short arrow denotes accommodating displacements of the outer strands, β9. (b) The four outer β-strands, as viewed from the external surroundings. The inner and outer β-strands have blue and red labels, respectively; the trace colours are: α, black; β, pink; γ, red; δ, purple.

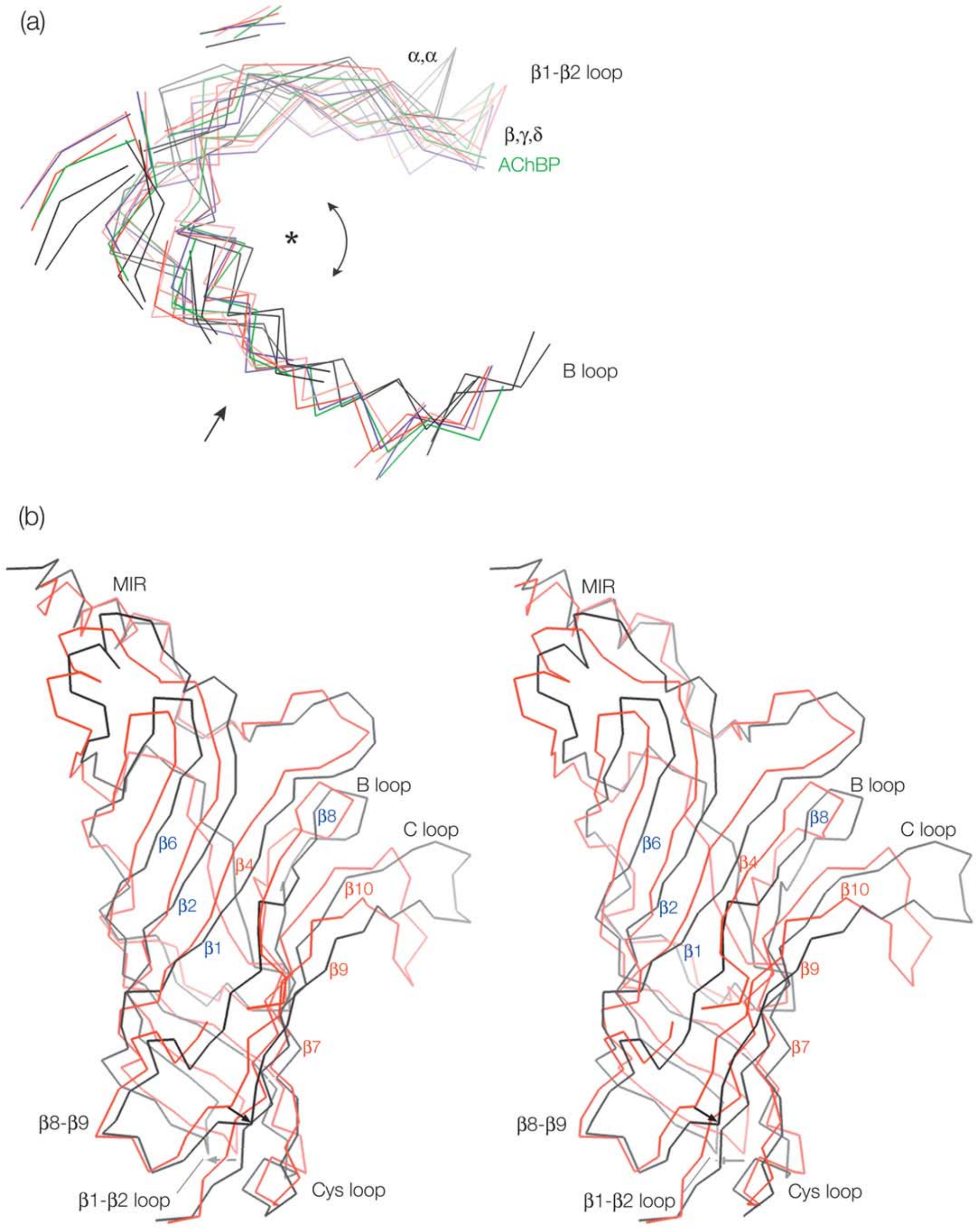

Figure 11. Comparison of α and non-α subunits in the ligand-binding domain, as in Figure 10, after translational alignment of the inner β-sheets to a common rotation axis (asterisk). (a) The projected backbone traces of the five sets of inner sheets (including the β1–β2 loops and the equivalent region of AChBP), as viewed from the synaptic cleft. (b) A stereo view (from the direction of the oblique arrow in (a)) comparing α with a non-α subunit (γ) over the whole β-sandwich domain; inner and outer β-strands are identified with blue and red labels, respectively; the arrows near the bottom of the Figure denote displacements of β-strands in α relative to non-α (see also Figure 10(a)). The colours are: α, black; β, pink; γ, red; δ, purple; AChBP, green.

extremes. These disparities reflect a small difference in twist between the β9–β10 hairpins of the α and non-α subunits (∼10° over 20 Å). The β9–β10 hairpin of the α subunit is less twisted, diminishing the overall (right-handed) twist of the outer sheet. The "untwisting" causes the β9 strand of α to be displaced outwards at the level of the disulphide bridge (short arrow, Figure 10(a)), creating the space that is needed to accommodate the anticlockwise-rotated inner sheet.

Refinement of rotation axis

It had been proposed that the α subunits in the closed channel were in a "distorted" configuration relative to the others and that the conformational change to open the channel involved movements that brought them into a configuration similar to that of the non-α subunits, making the whole assembly more symmetrical.[18] The rotational movements of the inner sheets played a key role in this mechanism, because of their close association (through the loop β1–β2) with the pore-lining M2 helices. It is therefore of interest to establish the location of the true axis of rotation within the protein subunit. This does not have to pass exactly through the disulphide bridge, provided that the cysteine residue (αC128) associated with the inner strand (β6) and the cysteine residue (αC142) associated with the outer strand (β7) undergo similar small displacements.

To define a common axis, we determined the translations that minimised the rms deviations between the C^{α} coordinates of the five sets of inner sheets. Following alignment by this criterion, the sheets superimposed tightly on the same semicircular arc (Figure 11(a)), with the α subunits clearly belonging to one group and the non-α subunits to another (values of $\mathrm{rmsd}_{C^{\alpha}}$ with respect to α_{γ} were: $\alpha_{\delta}=0.7$ Å; $\beta=2.1$ Å; $\gamma=2.2$ Å and $\delta=2.2$ Å). Pairwise least-squares analyses of different α and non-α combinations then yielded similar locations for the rotation axis, which were centred 8–9 Å from the midpoint position relating to the disulphide bridge (Figure 10(a)). We interpret the line passing through this point (Figure 11(a)), and normal to the membrane, to be the best estimate of the true axis of rotation. The line extends through the hydrophobic core of the ligand-binding domain, the base of the β9–β10 hairpin and between helices M1, M3 and M4, forming the outer protein shell of the membrane-spanning domain (Figure 9(a)).

Figure 11(b) compares the α subunit with a non-α subunit (γ), after this alignment, in the context of the whole β-sandwich domain. As indicated in Figure 10, the anticlockwise-rotated strands of the α inner sheet (grey arrow) are complemented by an outward displacement of the strand β9 of the outer sheet (black arrow), near the "bottom" of this domain.

ACh-binding region

The β9–β10 hairpin of the α subunits incorporates the C loop, which is implicated in ACh binding. The C loop is resolved only weakly in both α subunits, suggesting it is flexible in the absence of ACh. Densities are not visible for residues 191–194 in α_{δ}, but are present in the equivalent part of α_{γ}, possibly because in the crystal lattice the C loop of α_{γ} is next to the C loop of an adjacent subunit (see Figure 1), which stabilises its conformation. Figure 12 shows the C loop of the α_{γ} subunit and the neighbouring region, with the polypeptide backbones and interpreted side-chain positions superimposed on the experimental densities. The labelled side-chains Y190, Y198, C192 of the C-loop and W149 of the B loop are conserved in ACh receptor α subunits and co-ordinate to the bound ACh analogue, carbamylcholine, in the complex with AChBP.[9] Thus this whole region, including the A loop (not visible in the Figure) and the adjacent strands β5 and β6 of the γ (or δ) subunit, is involved in shaping the ACh-binding pocket of the receptor.

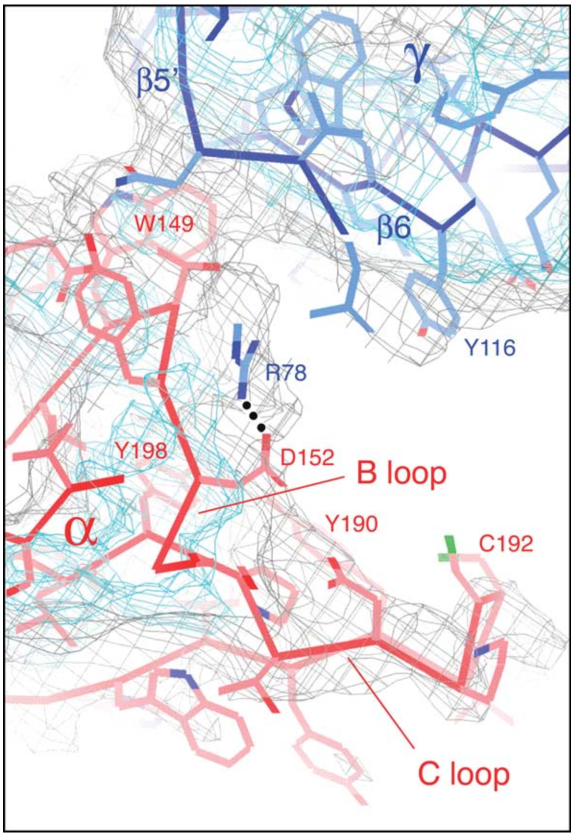

Figure 12. Interpretation of the ACh-binding region of the closed channel at the interface between the α and γ subunits, showing the loops B and C (α subunit), the adjacent strands, β5 and β6 (γ subunit) and the attached amino acid side-chains. The slab is of the upper part of the ACh-binding region, viewed from the synaptic cleft. Some key residues implicated in ACh binding are labelled. The C^{α} backbone and side-chains are in red (α) and blue (γ). As indicated, a salt-bridge between αD152 and γR78 may be involved in stabilising the B loop. The superimposed experimental densities show weak features associated with the C loop; contours at 2.0σ (grey) and 3.0σ (cyan).

In lower resolution studies of the ACh receptor,[13,14] we had found that the α subunits differed most from the non-α subunits, not at the interface region shown in Figure 12, but closer to the centre of the β-sandwich. Both α subunits displayed weaker densities at the centre of the sandwich, indicating that they had a more open structure there than did the other subunits, so we had identified the central region as the "putative ACh-binding site". It is evident now from the refined structure that the more open appearance is a consequence of the distinct inner- and outer-sheet arrangements in the α subunits. The β9–β10 hairpin of the α subunits, for example, is ~1.5 Å further from the oppositely facing inner β2 and β6 strands than it is in the other subunits at the level of the binding sites. Clearly, the earlier identification was mistaken, and the actual binding sites are closer to the γ and δ-subunit interfaces in locations equivalent to those in AChBP.[6,9]

As Figure 12 shows, the C loop projects away from the body of the α subunit in the closed-channel form of the receptor. This is in contrast with (ligand-bound) AChBP, where the C loop projects approximately tangential to the central 5-fold axis,[9] and so is closer to the A and B-loop residues implicated in ACh binding. The C^{α} distance between C192 (C loop) and W149 (B loop), for example, is 12 Å in AChBP, compared with 18 Å in the receptor. These loops must therefore undergo quite large relative movements in order to allow coordination of the binding residues to the ACh molecule: a conclusion consistent with biochemical results implying that the C-loop cysteine residues (C192, C193) move in a few ångström units toward a negative subsite when agonist binds.[35]

The involvement of the B loop in this local rearrangement is likely to be critical because it joins the outer to the inner β-sheets and therefore must participate directly in effecting their relative displacements, which leads to opening of the channel (see Discussion). The B loops of the α subunits come close to the inner β5 and β6 strands of the γ and δ subunits and so may be stabilised in the closed channel by interactions across the subunit interface. One example is a possible salt-bridge between αD152 and γR78 or δR81 (Figure 12), but there are several other potential contacts with the γ or δ subunits in this region (Figure 6).

Comparison with AChBP

Each of the subunits in the ligand-binding domain has a hydrophobic core of conserved residues which are grouped into three clusters, as in the protomer of AChBP.[6] The core residues of the receptor (pink background, Figure 5) are equivalent to those identified in AChBP, with the exception of the leucine (αL6) near the end of the N-terminal α-helix. Several hydrophobic residues not identified in AChBP also contribute to the core in the receptor. These residues are conserved among the nicotinic subunits and align with αV33, αL56, αI78, αL80, αL108, αW118 and αF124. The overall matching follows the predicted pattern of inward and outward-facing residues,[6,36] confirming that the core three-dimensional structures of all the pentameric subunits are essentially the same.

Furthermore most of the surface loops correlate closely between the two structures, even in regions where the amino acid sequences are not conserved. The hydrophobic Cys loop of the receptor, for example, has a similar fold to its hydrophilic counterpart in AChBP, but for the insertion of the extra residue in the receptor. The insertion extends the "heel" on the foot-shaped loop (Figure 4(a)), so that the loop straddles more completely the M2–M3 linker of the membrane-spanning domain. However, the stretch β5–β5′ (aligning with αV103–αM105) of the ligand-binding domain is significantly different from its counterpart in AChBP, folding inwards toward the core of the subunit. The binding site residue αW149 is thereby exposed more fully to the lumen of the vestibule (Figure 3(a)). Portions of the β8–β9 loops of the β, γ and δ subunits have no counterpart in AChBP, but these regions are also missing from the receptor structure.

AChBP does not have an equivalent of the MIR, a special region at the extreme extracellular end of the α subunits[37] that constitutes the major binding site for antibodies in the auto-immune disease, myasthenia gravis.[38,39] The critical segment of the epitope of these antibodies has been localised to residues αW67–αD71 (red letters, Figure 5), with αN68 and αD71 contributing most to the antigenicity.[39,40] This five-residue segment forms a loop apparently having the same β-folded structure (Figure 2(c)) as was found in NMR studies of peptide–antibody complexes.[41] All five residues (including the conserved core residue αW67) appear to be exposed to solvent because of the wide separation between the loop and the N-terminal helix. The equivalent loops of the other subunits have the same fold, but are closer to their respective helices (Figure 11(b)), which at least partly bury the inward-facing residues aligning with αW67 and αD71.

Discussion

The refined 4 Å structure reported here provides a chemical interpretation of all the main functional regions of the ACh receptor, as they would appear under near-physiological ionic conditions in *Torpedo* postsynaptic membranes. Although the final crystallographic *R*-factor was only 36.7%, limited by the quality of the amplitudes from images, we demonstrated that the polypeptide chains could now be traced with reasonable confidence over the entire length of the molecule (Figures 2 and 12). This included the extreme extracellular and intracellular ends (at high and low tube radius), which were the parts most affected by errors inherent in the helical analysis. It was also possible to use comparisons between the experimental phases and the phases from calculated helical structures (Table 1) to identify and correct for deficiencies in the original data and to validate the agreement between the atomic model and the experimental density map. Such comparisons were not feasible in the lower resolution investigations of the whole molecule. The present interpretation is therefore both more accurate and more detailed than previously, and should furnish a preliminary three-dimensional framework to guide our understanding of the functional properties of this ion channel and of others in the superfamily.

In a recent structural analysis of the membrane-spanning portion of the receptor, we described the arrangement of α-helical segments encircling the (closed) ion-conducting pore,[10] and suggested how the extended conformational change initiated by ACh opens the gate of the channel through rotational movements communicated along the pore-lining helices. The present study complements that analysis focused on the gate and the membrane pore, providing now a description of the structure around the ACh-binding site. The binding site in the closed channel differs considerably from that in AChBP, where ligand is present, indicating that the binding reaction is accompanied by a localised structural rearrangement. Comparison with AChBP shows that the localised changes blend naturally with the larger-scale structural changes, yielding a simple explanation (discussed below) for how the binding reaction is used to drive the extended conformational change. Given the improved understanding of this initial step, it is now possible to sketch a complete picture of the series of coordinated events leading to opening of the channel.

Special conformation of the α subunits

Our analysis of the ligand-binding domain confirmed that the subunits of the closed channel have two alternative extended conformations: one characteristic of either α subunit, and the other characteristic of the three non-α subunits.[18] However, the refined structure enabled more accurate measurement of their differences. We determined that the inner sheets of the β-sandwich composing this domain are rotated by approximately 10° in both α subunits relative to the non-α subunits (i.e. about 5° less than estimated earlier), about an axis normal to the membrane plane. We determined that the rotation axis lies 8–9 Å from the Cys-loop disulphide bridge, so that it passes almost centrally between the ends of helices M1, M3 and M4 forming the outer protein shell of the membrane-spanning domain (Figure 9(a)). We also observed, as before, that the outer sheets of the β-sandwich have slightly different orientations in the α compared with the non-α subunits (Figure 10(c)), and were able to show in this study that the β9–β10 portion of the α outer sheets has a reduced twist.

Several interactions across the subunit–subunit interfaces were identified that might be involved in stabilising the special conformation of the α subunits. These occur on both sides of both α subunits and implicate residues on the B loop as well as on the inner β-sheets. Salt-bridges are likely to be important, since they are present only at interfaces made with the α subunits. The "untwisted" configuration of the β9–β10 hairpin may be stabilized through an additional set of interactions unique to the α subunits: possibly through a salt-bridge between D200 on β9–β10 and K145 on β7 at one end, and a hydrophobic contact between αI210 on β9–β10 and the Cys loop at the other end (see Figure 9(b)). Since these inter and intra-subunit interactions are similar, or the same, for both α subunits, one would expect their three-dimensional structures to be the same. With the exception of differences at the binding site (where the C loop of α_δ is disordered), and of variations in side-chain conformations (which could not be resolved), this seemed to be the case.

Local rearrangement associated with ACh binding

We call the special conformation of the α subunits a "distorted" conformation because these subunits convert to a conformation similar to that of the non-α form, and of (ligand-bound) AChBP, when the channel is opened by ACh.[18] It is as if the α subunits are held initially in a distorted (or tense) state, by the interactions just described, and the energy of binding overcomes the distortions, allowing the α subunits to convert toward the (relaxed) non-α form that they would have if these interactions did not exist (in analogy with other allosteric proteins).[42] By comparing the binding site region of the α subunit (having no ligand present) with the corresponding region of AChBP (having ligand bound) we can obtain insight into how the local disturbance associated with the binding reaction drives the movements that overcome the distortions, allowing the α subunits to relax. AChBP provides a close analogue of the binding site in the receptor,[43] although the C loop of the α subunit has an extra residue at P197. In particular, both proteins contain the same set of aromatic residues, which arrange in a tight "box" around the quaternary ammonium group of the bound molecule.[9]

Figure 13(a) and (b) give simplified representations of the binding-site region shown in Figure 12 and the equivalent region of AChBP to which the ACh analogue, carbamylcholine is bound.[9] Comparison of these free and ligand-bound structures shows that the B and the C loops would both close in around the ACh molecule to enable coordination of the relevant side-chains: the B loop by rotating clockwise (large arrow) and the C loop by a twisting and rotating movement (small arrows). The A loop (not shown) would also be involved, but the indicated movements are smaller.

The AChBP protomer can be aligned translationally to the rotation axis relating the inner β-sheets of the receptor, after optimal superposition of the pentamers, and thereby identified unequivocally with the non-α conformation (Figure 11(a)). Such an alignment also allows a realistic superposition of the protomer with the α subunit to simulate how the local rearrangement would be communicated to the β1–β2 loop (and from there to the gate in the membrane). As Figure 13(c) shows, the B loop is joined to strand β8 of the inner sheet, and the inner sheet itself would act as a rigid connecting link, transmitting the clockwise rotation initiated at the B loop to the β1–β2 loop on the opposite face of the subunit. Alternatively the change (pink to green) can be regarded as a conversion from the distorted to the (relaxed) non-α form of the subunit. The implication is therefore that the ACh-binding

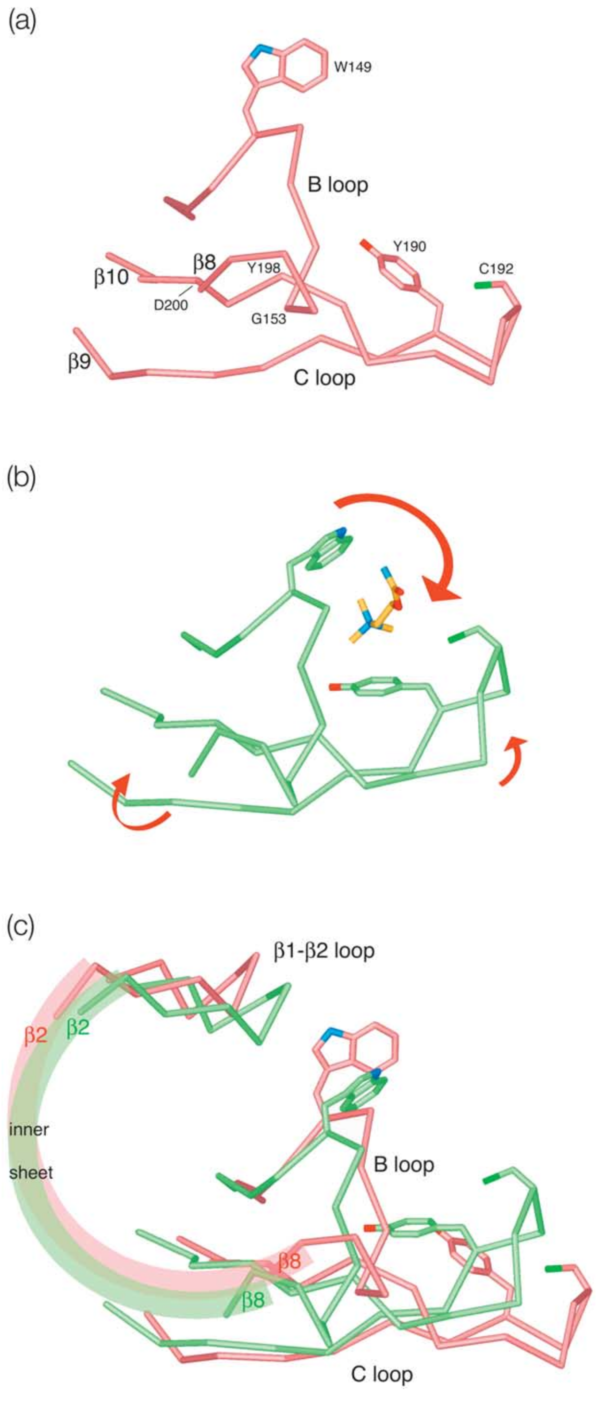

Figure 13. Comparison of the ACh-binding region in the α subunit with ligand-bound AChBP[9] suggests how the local rearrangement caused by ACh initiates the extended conformational change to open the channel. The Figure shows: (a) simplified C^{α} traces of the ligand-binding region of the α subunit, with labels identifying parts mentioned in the text; (b) the equivalent region of AChBP complexed with carbamylcholine (PDB entry 1UV6); (c) the two regions superimposed after alignment to a common rotation axis (Figure 11(a)), and extension to include the two β1–β2 loops, which are connected to the B loops through the inner sheets (arcs). The α subunit is in the closed-channel conformation, whereas AChBP is an analogue of the open or desensitised state.[76] Closure of the B and C loops around the bound agonist changes the orientation of the B loop (large arrow in (b)) and twist of the β9–β10-hairpin (twisted arrow in (b)). It is proposed that these changes together drive the clockwise rotations of the inner sheets, favouring the open-channel extended conformation.

reaction would drive the movements to open the channel by initiating a local rearrangement that makes the non-α conformation more stable.

Several of the residues participating in the local rearrangement may play key roles in enabling the larger scale movements, and hence in coupling the binding reaction to opening of the channel. The glycine residue αG153 (Figure 13(a)), for example, may help in conferring flexibility on the B loop as would be needed to enable the linked movements of the inner sheets. The mutation αG153S is in fact a naturally occurring mutation, causing a slow channel congenital myasthenic syndrome in which the channel reopens more readily than in the wild-type.[44,45] The aspartic acid residue αD200 (Figure 13(a)), through interaction with strand β7, may help in constraining the twist of the β9–β10 hairpin in either of the alternative conformations. The mutation αD200N is another well-characterised mutation that leads to impaired gating of the channel.[46,47] Mutations of the A, B and C-loop residues αY93, αW149, αY190 and αY198, which interact directly with bound ligand in AChBP,[9] also affect gating.[48–51]

Propagation of the conformational change

The conversion of the α subunits to a non-α-like conformation is the major extended conformational change controlling channel opening, according to the structural differences revealed in receptors briefly exposed to ACh.[17,18] As analysed here, the transition would involve mainly rigid-body movements of the inner and outer-sheet parts of the β-sandwich and small rearrangements or readjustments by the connecting loops. The inner sheet would be the primary structural element determining the gating function of the channel, making use of a rotational movement to effect a displacement of the β1–β2 loop next to the helix lining the membrane pore; whereas the outer sheet would provide the structural framework needed to initiate the rotational movement and to accommodate the displacements involved. At the same time, disturbance of the neighbouring subunits would be minimised by having the rotation axis normal to the membrane plane.

The twist of the α-subunit β9–β10 hairpin seems likely to play an important role in coordinating these movements. We showed that it is "untwisted" in the closed channel, creating room for the inner sheet to be in the rotated-anticlockwise position (Figure 10(a)). In the open-channel, it would be "twisted", as in a non-α subunit, fitting (together with the β8–β9 loop) against the inner sheet in the rotated-clockwise position. Because of the complementary nature of changes such as these, the relative displacements between the inner and outer parts of the β-sandwich, in the interior of the subunit, would be quite small. In fact, no fundamental difference was detected between the α and non-α subunits in their interior organisation, suggesting that the relative displacements would be accommodated through minor adjustments in torsion angles of the inward-facing side-chains.

Coupling to the membrane

How do the rotational movements in the ligand-binding domain communicate through the M2 helices to open the channel? The limited resolution of this study, the absence of a high-resolution structure of the open channel and the limited information available from mutagenesis studies[52,53] do not yet allow a definitive answer. However, the structure suggests that the β1–β2 and the Cys loops may together influence M2–M3 at either ends to control the gating movements. The β8–β9 loop is also implicated[54–56] (Figure 10(a)), but it does not extend to the membrane-spanning domain.

One possibility is that the fast gating of the M2 helices, in the absence of a ligand-binding domain, would be analogous to that of M2 peptides in lipid bilayers, which open and close constitutively like the authentic channels,[57] and that these motions are disallowed by the α subunits in their closed-channel conformation. The β1–β2 and Cys loops are 2–3 Å closer to the end of M2, along the M2–M3 linker, in the α than in the non-α subunits (Figure 9(a)). In these locations they might respectively lock M2 in its closed configuration and restrict the flexure of M2–M3 conferred by the conserved glycine residue (αG275) at the end of M3 (Figure 9(b)). When ACh binds and the loops rotate back toward their non-α locations, these restrictions could be relieved, allowing the fast gating motions to occur.

A displacement of the two loops over M2–M3 is consistent with the change in accessibility during gating of the residue α_1A284 of the GABA$_A$ receptor,[58] since this residue (aligning with αL273[1]) lies between the β1–β2 and Cys loops on M2–M3. However, an alternative possibility is that the specific interaction involving αV46 on the β1–β2 loop is maintained, and that the loop movement promotes opening of the pore by drawing the end of M2 away from the axis of the channel. Whatever the precise nature of the coupling, the fast gating kinetics implies that the activation energy required to switch between the open and closed pores is very small. Only a minor structural perturbation should therefore be sufficient to tip the balance one way or the other.

Coordinated gating movements

The opening and closing of the ACh receptor channel is usually regarded as a concerted process, whereby the whole protein switches rapidly between alternative "pre-existing" conformations.[59] It may also be considered in terms of a "conformational wave".[60] However, it is better understood mechanistically if the action is broken down into a series of coordinated events. The structural details described above, and previous results focusing on the membrane pore,[10] now provide a complete (simplified) model for the series of coordinated events leading to opening of the channel. The steps would be: (a) ACh enters the two binding sites, causing loops B and C of the α subunits to close in around the bound molecule; (b) the resulting local rearrangement reduces the stability of distorted form of the α subunits in favour of the relaxed (non-α) form; (c) the extended conformational change is therefore initiated, displacing the β1–β2 loops of α over the ends of their respective M2 helices; (d) the displacements unlock the interactions that restrict the rotational movements of the pore-lining helices; (e) the helices move, destabilising the weak hydrophobic interactions holding the gate together, so that it breaks apart.

Our results imply the α subunits are the principal mediators of the conformational change that opens (or closes) the channel, whereas the other subunits contribute critically in influencing ACh binding and in stabilising closed-channel conformation of the α subunits so that they can make the appropriate response. In addition, a clear distinction can be drawn between the movements in ligand-binding domain and in membrane-spanning domain, where the structure is more symmetrical and the subunits contribute equally to the opening sensitivity of the pore.[26] The gating appears to occur by fast cooperative movements of helices lining the membrane pore, while the ligand-binding domain may function as a controlling device that either disenables or facilitates these movements.

Ion selectivity and conductance

The three-dimensional structure reveals a scattered distribution of charged groups lining the inner walls of both vestibules (Figure 8), and so highlights the fact that it is the overall effect of many side-chains that gives rise to the electric fields that would influence ion flow through the narrow membrane pore. This picture complements the findings of mutagenesis combined with electrophysiological experiments, where the focus is directed at individual side-chains.

Mutagenesis experiments have shown, for example, that the cation conductance of the muscle-type ACh receptor is strongly diminished by reduction of the negative charge of the "inter-intermediate" ring (at αE241 in Figure 8(b)) near the intracellular end of M2.[21] Also ion selectivity of the α7 ACh receptor was changed from cationic to anionic by altering the charge on this ring, inserting a proline next to it and substituting a residue in the pore.[61] Similar changes in ion selectivity have been observed with other members of the superfamily on changing the equivalent amino acid residues near the intracellular end of M2.[62,63] Consequently, this

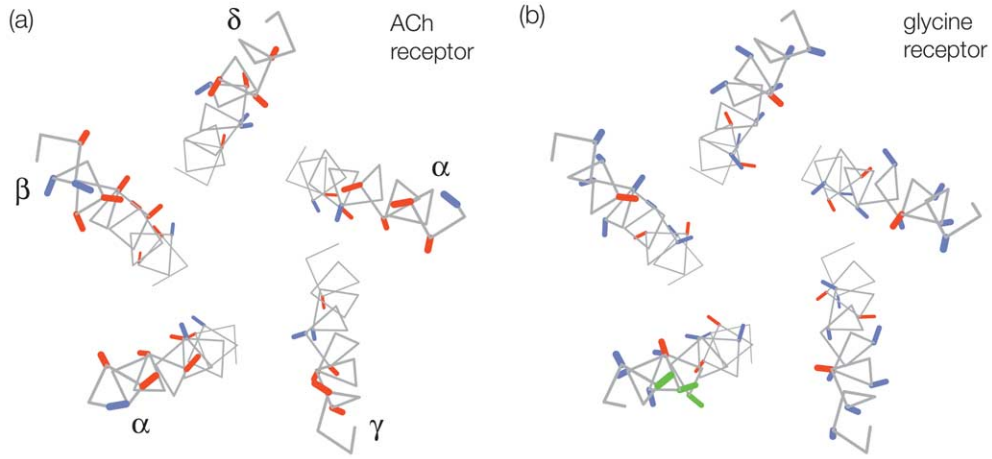

Figure 14. Distribution of charged residues on MA helices shaping the intracellular vestibules of transmitter-gated ion channels: (a) as found in this study for a cation-selective channel; (b) homology model of MA helices of a related anion-selective channel (human glycine receptor α1 subunits; amino acid residues 369–394). The panels show C^{α} traces, with bars denoting the C^{α}–C^{β} bonds of residues having negative (red) or positive charge (blue); the view is from the synaptic cleft. In (a) the inside of the vestibule and the windows for the ions are lined predominantly by negatively charged groups, whereas in (b) the opposite distribution applies. Also shown on one of the helices in (b) are the locations in the (cation-selective) 5-HT_{3A} receptor of three arginine residues (green bars); the single-channel conductance increases dramatically when these residues are mutated to neutral or negatively charged residues.[65]

local region is sometimes referred to as the charge selectivity filter of the channel.[64] Yet the unperturbed three-dimensional structure of the ACh receptor shows numerous negatively charged groups within the same confined space (Figure 8(b)). Evidently, the residues identified by mutagenesis are supplemented by many others to create the electrostatic environment that is required for efficient cation-selective transport.

The importance of the intracellular vestibule is underlined by the fact that the equivalent regions in anion-selective members of the superfamily have opposite distributions of charge. Figure 14 compares the MA helices of the ACh receptor with those of the (anion-selective) homomeric glycine receptor, after homology alignment. In one case (ACh receptor; Figure 14(a)) the inside of the vestibule is lined predominantly by negatively charged groups; in the other (glycine receptor; Figure 14(b)) it is lined predominantly by positively charged groups. Thus the whole inner surface of the vestibule contributes either a cation-stabilising or an anion-stabilising environment, depending on the type of transmitter-gated channel.

The narrowest region of the membrane pore, determining ion flow through the ACh receptor, is at the intracellular end of M2 near αT244.[22] But the lateral windows of the intracellular vestibule are equally, if not more constricting, and in other channels may restrict the total flux to the extent that they play a rate-limiting role. Evidence that this does occur has been obtained recently by combined mutagenesis and electrophysiological experiments on (cation-selective) 5-HT_3 receptors.[65] The single channel conductance of the recombinant homomeric 5-HT_{3A} receptor was <1pS, but co-expression with the 5-HT_{3B} subunit increased the conductance more than 40-fold. The poor conductance of the homomeric channel was attributable to three arginine residues, which align with the window-framing residues of the receptor (green bars; Figure 14(b)). Mutation of the arginine residues in the 5-HT_{3A} receptor to their neutral or negatively charged 5-HT_{3B} counterparts overcame the anomalously low conductance of the homomeric channel, as the structure would predict.

Therefore, while the intracellular vestibule of the ACh receptor appears to function primarily as an electrostatic filter, screening out ions of the wrong charge and size, in other members of the superfamily it may have the additional role, related to the particular subunit combination, of determining the conductance of the channel.

General conclusions

This analysis extends earlier electron microscopic analyses of the ACh receptor in *Torpedo* postsynaptic membranes, imaged either in the absence of ACh, or following brief exposure to ACh to trap the open-channel form. The results together suggest that the channel has the following properties that are fundamental to the way it works:

The main ligand-binding α subunits, in the closed channel, are in a "distorted" state, which is stabilised by inter and intra-subunit interactions.

In the conformational change to open the channel, the main ligand-binding subunits are the principal mediators, leading to a concerted rearrangement in the membrane involving all the helices lining the pore.

The bound ACh opens the channel by causing a localised rearrangement that stabilises the alternative "relaxed" conformation of the ligand-binding subunit.

The transition to the open state involves rotational movements in the ligand-binding subunits, which unlock their interactions with the pore-lining helices keeping the channel closed.

The gating movements are quite small, being restricted energetically by the need to preserve the conserved hydrophobic cores of the subunits.

The ionic surfaces of the vestibules play an important role in facilitating the selective transport of cations through the channel.

The high level of amino acid sequence conservation, and the functional specificities able to be achieved with chimeric channels,[56,66] imply that all channels of the Cys-loop superfamily are constructed around the same three-dimensional framework and function according to the same global principles. These principles applying to the ACh receptor are therefore likely to apply, with minor variations, to other members of the superfamily.

Methods

Model building

The amino acid sequences of the four *T. marmorata* polypeptide chains[67,68] were used to create the starting receptor structure for the refinement. This structure was modelled initially by fitting fragments of the chains to the experimental densities using the program O.[32] The membrane-spanning region was modelled from the original coordinates (PDB entry 1OED). The extracellular region was modelled from the coordinates of the separately aligned inner and outer β-sheet fragments of AChBP,[18] omitting at this stage the N-terminal α-helix and most of the connecting loops. The pentagonal structure shaping the intracellular vestibule was built from stretches of the amino acid sequence that had been tentatively identified with this part of the receptor,[14] but which could not until now be fitted convincingly to the densities. Further stretches of polypeptide were built into the model at later stages in the refinement. In the case of the extracellular region, these stretches included the N-terminal α-helix, the MIR, the C loop, the Cys loop and the remaining connecting links. In several parts of the map, where the densities could not be interpreted unambiguously, the chains were built into the model assuming the fold most closely matching that of the related region in AChBP or in another subunit. No significant densities were found that might correspond to ordered lipid molecules or oligosaccharides attached to extracellular portions of the subunits.[69]

Three-dimensional density map

The 4 Å map on which the refinement was conducted had been derived as a weighted average of the densities representing a single receptor, determined from four helical families of tube ((−16,6); (−17,5); (−15,7); (−18,6)).[10] In each family, the densities were determined by combining the Fourier terms from the images along ∼1500 layer-lines, and imposing the symmetry consistent with the p2 surface lattice. The criterion for inclusion of Fourier terms in the data sets was based on signal-to-noise measurement at each point along each layer-line, or Point Quality (PQ):

$$\mathrm{PQ}(R,l) = \sqrt{2F(R,l)^2\cos^2(\delta\phi)/\mathrm{BKG}(R,l)^2}, \quad \mathrm{PQ}(R,l) \geq 1$$

where F is the amplitude of the Fourier term at radius R along the layer-line l, $\delta\phi$ is the deviation of its phase from the nearest of 0° or 180°, and BKG is the measured background amplitude.[33] No additional editing of individual layer-lines or solvent flattening[70] was performed.

Helical structures and phase comparisons

Structures representing each helical family (i.e. having the same symmetry elements and average unit cell dimensions) were built from the coordinates of the modelled receptor using the program HLXBLD (written by M. Stowell). Helical transforms were then calculated from the tube structures to yield the continuous variations in amplitude and phase along layer-lines located at multiples of the helical repeat. The phase variations along the layer-lines, calculated in this way, should ideally match the phase variations along the same layer-lines obtained from the Fourier transforms of the images. In practice, however, the presence of noise prevents perfect agreement from being achieved.

One important source of noise was the overlap of layer-lines and consequent mixing of Bessel terms having different orders.[14] This gave rise to spurious amplitudes that were weakened, but not entirely removed by the averaging. We describe below an objective method used to weaken the effect of spurious amplitudes by identifying and eliminating layer-lines where the amplitudes are dominated by noise. Application of this method brought about a significant improvement in the quality of the density map, as assessed by comparison between the measured and calculated phases (Table 1).

Treatment of noise along layer-lines

To distinguish layer-lines containing a weak signal from those containing no signal we measured the PQ and F/BKG values averaged over the first (strongest) portion of each layer-line (i.e. from $R = n/2\pi r_{\mathrm{max}}$ to $R = n/2\pi r_{\mathrm{min}}$, where n is the Bessel order, r_{max} and r_{min} are the outer and inner radii of the tube). We then selected layer-lines for retention based on the ratio of the mean values, $\Phi_{\mathrm{m}} = \bar{\mathrm{PQ}}/(\bar{F}/\bar{\mathrm{BKG}})$, i.e. the mean amplitude-weighted "Figure of merit". It can be shown that $\Phi_{\mathrm{m}} \approx 1.414$ (i.e. $\sqrt{2}$) for a strong layer-line, and 0.900 (i.e. $\sqrt{2(2/\pi)^2}$) for a layer-line containing only random terms. Figure 15 plots Φ_{m} *versus* $\bar{F}/\bar{\mathrm{BKG}}$ for layer-lines of the (−16,6) family. A conservative value of $\Phi_{\mathrm{m}} = 0.877$ for inclusion of the layer-lines resulted in ∼20% of them being eliminated from each data set, while the agreement between the measured and calculated phases in all four cases improved by 2–4%. We used this threshold figure in deriving the final density map.

Crystallographic refinement

Torsion angle refinement was performed in CNS[71] using maximum likelihood (amplitude target), after placing the isolated densities corresponding to a single receptor in a P1 orthogonal unit cell (Table 2). To facilitate measurement of, and correction for possible effects of tube flattening (see Results), the central axis of the receptor (which lies radially to the axis of the tube) was

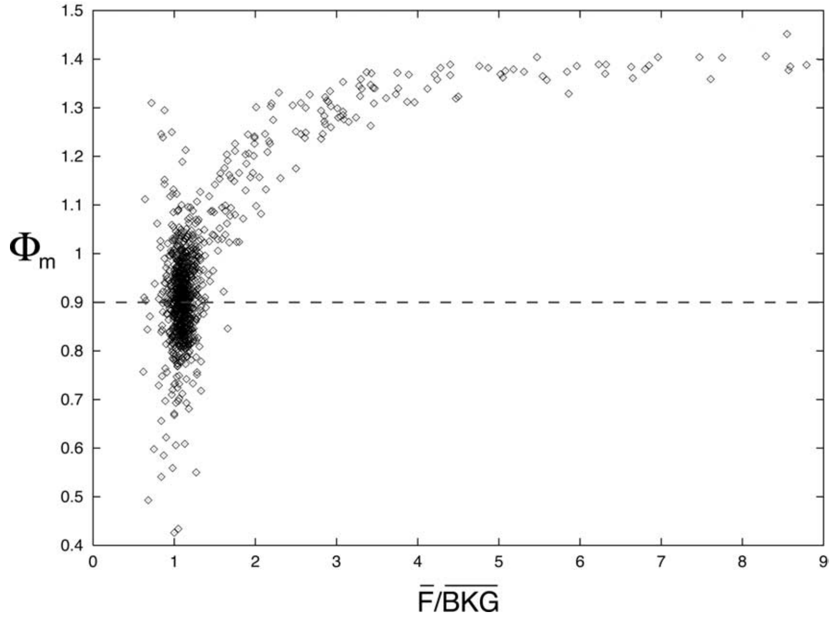

Figure 15. Φ_m plotted against $\bar{F}/\bar{BKG}$ for individual layer-lines of the (−16,6) helical family. The theoretical figure for Φ_m, assuming the layer-line contains only random terms, is 0.9 (broken line); layer-lines with $\bar{F}/\bar{BKG} > 9.0$ have not been plotted. See the text for details.

aligned with the *c* axis of the cell and overall anisotropic temperature factors were used. Atomic scattering factors for electrons were used without taking account of chemical bonding effects or charge. The *R*-factors were calculated over the range: 100–4 Å, with 5% of the terms being used for the calculation of R_{free}. Throughout the refinement, the value of R_{free} was monitored with parallel measurement of the helical phase residuals, obtained by comparing the experimental with calculated phases from structures of tubes. A reduction in R_{free} was considered valid only if it was not accompanied by an increase in the phase residual. The geometry of the final model was examined with the program PROCHECK.[72]

The Figures were prepared with the programs MOLSCRIPT,[73] SETOR[74] and GRASP.[75]

Atomic coordinates

The coordinates have been deposited in the Protein Data Bank with accession code 2BG9.

Acknowledgements

The structure refinement was based on data from electron images, all of which had been recorded in Japan using microscopes incorporating a liquid helium-cooled stage. I am particularly grateful to Yoshi Fujiyoshi, who designed the stage, and to Atsuo Miyazawa, who recorded most of the images, for their continued support and advice. The work has also benefited from many helpful discussions with colleagues at the Laboratory of Molecular Biology, Cambridge, UK, and at the Scripps Research Institute, La Jolla, CA, USA. The research was funded, in part, by grants from the European Commission (QLG3-CT-2001-00902) and NIH (GM61941).

References

1. Lester, H. A., Dibas, M. I., Dahan, D. S., Leite, J. F. & Dougherty, D. A. (2004). Cys-loop receptors: new twists and turns. *Trends Neurosci.* **27**, 329–336.
2. Colquhoun, D. & Sivilotti, L. G. (2004). Function and structure in glycine receptors and some of their relatives. *Trends Neurosci.* **27**, 337–344.
3. Absalom, N. L., Lewis, T. M. & Schofield, P. R. (2004). Mechanisms of channel gating of the ligand-gated ion channel superfamily inferred from protein structure. *Expt. Physiol.* **89**, 145–153.
4. Colquhoun, D., Shelly, C., Hatton, C., Unwin, N. & Sivilotti, L. (2003). Nicotinic acetylcholine receptors. *Burger's Med. Chem. Drug Discov.* **2**, 357–406.
5. Karlin, A. (2002). Emerging structure of the nicotinic acetylcholine receptors. *Nature Rev. Neurosci.* **3**, 102–114.
6. Brejc, K., van Dijk, W. J., Klaassen, R. V., Schurmanns, M., van der Oost, J., Smit, A. B. & Sixma, T. K. (2001). Crystal structure of an ACh-binding protein reveals the ligand-binding domain of nicotinic receptors. *Nature*, **411**, 269–276.
7. Corringer, J.-P., Le Novère, N. & Changeux, J.-P. (2000). Nicotinic receptors at the amino acid level. *Annu. Rev. Pharmacol. Toxicol.* **40**, 431–458.
8. Sine, S. M. (2002). The nicotinic receptor ligand binding domain. *J. Neurobiol.* **53**, 431–446.
9. Celie, P. H. N., van Rossum-Fikkert, S. E., van Dijk, J. W., Brejc, K. & Smit, A. B. (2004). Nicotine and carbamylcholine binding to nicotinic acetylcholine receptors as studied in AChBP crystal structures. *Neuron*, **41**, 907–914.
10. Miyazawa, A., Fujiyoshi, Y. & Unwin, N. (2003). Structure and gating mechanism of the acetylcholine receptor pore. *Nature*, **423**, 949–955.
11. Beckstein, O. & Sansom, M. S. P. (2004). The influence

of geometry, surface character, and flexibility on the permeation of ions and water through biological pores. *Phys. Biol.* **1**, 42–52.

12. Corry, B. (2004). Theoretical conformation of the closed and open states of the acetylcholine receptor channel. *Biochim. Biophys. Acta*, **1663**, 2–5.
13. Unwin, N. (1993). Nicotinic acetylcholine receptor at 9 Å resolution. *J. Mol. Biol.* **229**, 1101–1124.
14. Miyazawa, A., Fujiyoshi, Y., Stowell, M. & Unwin, N. (1999). Nicotinic acetylcholine receptor at 4.6 Å resolution: transverse tunnels in the channel wall. *J. Mol. Biol.* **288**, 765–786.
15. Brisson, A. & Unwin, P. N. T. (1984). Tubular crystals of acetylcholine receptor. *J. Cell Biol.* **99**, 1202–1211.
16. Toyoshima, C. & Unwin, N. (1990). Three-dimensional structure of the acetylcholine receptor by cryoelectron microscopy and helical image reconstruction. *J. Cell Biol.* **111**, 2623–2635.
17. Unwin, N. (1995). Acetylcholine receptor channel imaged in the open state. *Nature*, **373**, 37–43.
18. Unwin, N., Miyazawa, A., Li, J. & Fujiyoshi, Y. (2002). Activation of the nicotinic acetylcholine receptor involves a switch in conformation of the α subunits. *J. Mol. Biol.* **319**, 1165–1176.
19. Giraudat, J., Dennis, M., Heidmann, T., Chang, J. Y. & Changeux, J.-P. (1986). Structure of the high affinity binding site for noncompetitive blockers of the acetylcholine receptor: serine-262 of the δ subunit is labeled by [^{3}H]chlorpromazine. *Proc. Natl Acad. Sci. USA*, **83**, 2719–2723.
20. Hucho, F. L., Oberthur, W. & Lottspeich, F. (1986). The ion channel of the nicotinic acetylcholine receptor is formed by the homologous helices MII of the receptor subunits. *FEBS Letters*, **205**, 137–142.
21. Imoto, K., Busch, C., Sakmann, B., Mishina, M., Konno, T., Nakai, J. *et al*. (1988). Rings of negatively charged amino acids determine the acetylcholine receptor channel conductance. *Nature*, **335**, 645–648.
22. Villarroel, A., Herlitze, S., Koenen, M. & Sakmann, B. (1991). Location of a threonine residue in the α-subunit M2 transmembrane segment that determines the ion flow through the acetylcholine receptor channel. *Proc. Roy. Soc. ser. B*, **243**, 69–74.
23. White, B. H. & Cohen, J. B. (1992). Agonist-induced changes in the structure of the acetylcholine receptor M2 regions revealed by photoincorporation of an uncharged nicotinic noncompetitive antagonist. *J. Biol. Chem.* **267**, 15770–15783.
24. Akabas, M. H., Kaufmann, C., Archdeacon, P. & Karlin, A. (1994). Identification of acetylcholine receptor channel-lining residues in the entire M2 segment of the α subunit. *Neuron*, **13**, 919–927.
25. Sine, S. M., Kreienkamp, H.-J., Bren, N., Maeda, R. & Taylor, P. (1995). Molecular dissection of subunit interfaces in the acetylcholine receptor: identification of determinants of α-conotoxin M1 selectivity. *Neuron*, **15**, 205–211.
26. Labarca, C., Nowak, M. W., Zhang, H., Tang, L., Deshpande, P. & Lester, H. A. (1995). Channel gating governed symmetrically by conserved leucine residues in the M2 domain of nicotinic receptors. *Nature*, **376**, 514–516.
27. Zhong, W., Gallivan, J. P., Zhang, Y., Li, L., Lester, H. A. & Dougherty, D. A. (1998). From *ab initio* quantum mechanics to molecular neurobiology: a cation-pi binding site in the nicotinic receptor. *Proc. Natl Acad. Sci. USA*, **95**, 12008–12093.
28. Grosman, C., Salamone, F. N., Sine, S. M. & Auerbach, A. (2000). The extracellular linker of muscle acetylcholine receptor channels is a gating control element. *J. Gen. Physiol.* **116**, 327–340.
29. Brisson, A. & Unwin, P. N. T. (1985). Quaternary structure of the acetylcholine receptor. *Nature*, **315**, 474–477.
30. Chang, H. W. & Bock, E. (1977). Molecular forms of acetylcholine receptor. Effects of calcium ions and sulfhydryl reagent on the occurrence of oligomers. *Biochemistry*, **16**, 4513–4520.
31. Hamilton, S. L., McLaughlin, M. & Karlin, A. (1977). Disulfide bond cross-linked dimer in acetylcholine receptor from *Torpedo californica*. *Biochem. Biophys. Res. Commun.* **79**, 692–699.
32. Jones, T. A., Zou, J.-Y., Cowan, S. W. & Kjeldgaard, M. (1991). Improved methods for building protein models in electron density maps and the location of errors in these models. *Acta Crystallog. sect. A*, **47**, 110–119.
33. Beroukhim, R. & Unwin, N. (1997). Distortion correction of tubular crystals: improvements in the acetylcholine receptor structure. *Ultramicroscopy*, **70**, 57–81.
34. Finer-Moore, J. & Stroud, R. M. (1984). Amphipathic analysis and possible formation of the ion channel in an acetylcholine receptor. *Proc. Natl Acad. Sci. USA*, **81**, 155–159.
35. Karlin, A. (1969). Chemical modification of the active site of the acetylcholine receptor. *J. Gen. Physiol.* **54**, 245s–264s.
36. Sine, S. M., Wang, H. L. & Bren, N. (2002). Lysine scanning mutagenesis delineates structural model of the nicotinic acetylcholine receptor ligand binding domain. *J. Biol. Chem.* **277**, 29210–29223.
37. Beroukhim, R. & Unwin, N. (1995). Three-dimensional location of the main immunogenic region of the acetylcholine receptor. *Neuron*, **15**, 323–331.
38. Lindstrom, J. M. (2000). Acetylcholine receptors and myasthenia. *Muscle Nerve*, **23**, 453–477.
39. Tzartos, S. J., Barkas, T., Cung, M. T., Mamalaki, A., Orlewski, P., Papanastasiou, D. *et al*. (1998). Anatomy of the antigenic structure of a large membrane autoantigen, the muscle-type nicotinic acetylcholine receptor. *Immunol. Rev.* **163**, 89–120.
40. Wahlsten, J. L., Lindstrom, J. M. & Cont-Tronconi, B. M. (1993). Amino acid residues within the sequence region alpha 55-74 of *Torpedo* acetylcholine receptor interacting with antibodies to the main immunogenic region and with snake alpha-neurotoxins. *J. Recept. Res.* **13**, 989–1008.
41. Orlewski, P., Marraud, M., Cung, M. T., Tsikaris, V., Sakarellos-Daitsiotis, M., Sakarellos, C. *et al*. (1996). Compared structures of the free nicotinic acetylcholine receptor main immunogenic region (MIR) decapeptide and the antibody-bound [A76]MIR analogue: a molecular dynamics simulation from two-dimensional NMR data. *Biopolymers*, **40**, 419–432.
42. Monod, J., Wyman, J. & Changeux, J.-P. (1965). On the nature of allosteric transitions: a plausible model. *J. Mol. Biol.* **12**, 88–118.
43. Le Novère, N., Grutter, T. & Changeux, J.-P. (2002). Models of the extracellular domain of the nicotinic receptors and of agonist- and Ca^{2+}-binding sites. *Proc. Natl Acad. Sci. USA*, **99**, 3210–3215.
44. Engel, A. G., Lambert, E. H., Mulder, D. M., Torres, C. F., Sahashi, K., Bertorini, T. E. & Whitaker, J. N. (1982). A newly recognised congenital myasthenic

syndrome attributed to a prolonged open time of the acetylcholine-induced ion channel. *Ann. Neurol.* **11**, 553–569.
45. Sine, S. M., Ohno, K., Bouzat, A., Auerbach, A., Milone, M., Pruitt, J. N. & Engel, A. G. (1995). Mutation of the acetylcholine receptor alpha subunit causes a slow-channel myasthenic syndrome by enhancing agonist binding affinity. *Neuron*, **15**, 229–239.
46. O'Leary, M. E. & White, M. M. (1992). Mutational analysis of ligand-induced activation of the *Torpedo* acetylcholine receptor. *J. Biol. Chem.* **267**, 8360–8365.
47. Akk, G., Sine, S. & Auerbach, A. (1996). Binding sites contribute unequally to the gating of mouse nicotinic D200N acetylcholine receptors. *J. Physiol. (London)*, **496**, 185–196.
48. Auerbach, A., Sigurdson, W., Chen, J. & Akk, G. (1996). Voltage dependence of mouse acetylcholine receptor gating: different charge movements in di-, mono- and unliganded receptors. *J. Physiol. (London)*, **494**, 155–170.
49. Akk, G. (2001). Aromatics at the murine nicotinic receptor agonist binding site: mutational analysis of the αY93 and αW149 residues. *J. Physiol. (London)*, **535**, 729–740.
50. Chen, J., Zhang, Y., Akk, G., Sine, S. & Auerbach, A. (1995). Activation kinetics of recombinant mouse nicotinic acetylcholine receptors: mutations of α-subunit tyrosine 190 affect both binding and gating. *Biophys. J.* **69**, 849–859.
51. Akk, G., Zhou, M. & Auerbach, A. (1999). A mutational analysis of the acetylcholine receptor channel transmitter binding site. *Biophys. J.* **76**, 207–218.
52. Kash, T. L., Jenkins, A., Kelley, J. C., Trudell, J. R. & Harrison, N. L. (2003). Coupling of agonist binding to channel gating in the $GABA_A$ receptor. *Nature*, **421**, 272–275.
53. Absalom, N. L., Lewis, T. M., Kaplan, W., Pierce, K. D. & Schofield, P. R. (2003). Role of charged residues in coupling ligand binding and channel activation in the extracellular domain of the glycine receptor. *J. Biol. Chem.* **278**, 50151–50157.
54. Leite, J. F., Blanton, M. P., Shahgholi, M., Dougherty, D. A. & Lester, H. A. (2003). Conformation-dependent hydrophobic labelling of the nicotinic receptor: electrophysiology-coordinated photochemistry and mass spectrometry. *Proc. Natl Acad. Sci. USA*, **100**, 13054–13059.
55. Newell, J. G. & Czajkowski, C. (2003). The $GABA_A$ receptor α_1 subunit Pro^{174}-Asp^{191} segment is involved in GABA binding and channel gating. *J. Biol. Chem.* **287**, 13166–13172.
56. Bouzat, C., Gumilar, F., Spitzmaul, G., Wang, H.-L., Rayes, D., Hansen, S. B. *et al*. (2004). Structural network coupling agonist binding to channel gating revealed by ACh-binding protein linked to ion channel. *Nature*, **430**, 896–900.
57. Montal, M. O., Iwamoto, T., Tomich, J. M. & Montal, M. (1993). Design, synthesis and functional characterisation of a pentameric channel protein that mimics the presumed pore structure of the nicotinic cholinergic receptor. *FEBS Letters*, **320**, 261–266.
58. Bera, A. K., Chatav, M. & Akabas, M. H. (2002). $GABA_A$ receptor M2–M3 loop secondary structure and changes in accessibility during channel gating. *J. Biol. Chem.* **277**, 43002–43010.
59. Changeux, J. P. & Edelstein, S. J. (1998). Allosteric receptors after 30 years. *Neuron*, **21**, 959–980.
60. Grosman, C., Zhou, M. & Auerbach, A. (2000). Mapping the conformational wave of acetylcholine receptor gating. *Nature*, **403**, 773–776.
61. Galzi, J.-L., Devillers-Thiery, A., Hussy, N., Bertrand, S., Changeux, J.-P. & Bertrand, D. (1992). Mutations in the channel domain of a neuronal nicotinic receptor convert ion selectivity from cationic to anionic. *Nature*, **359**, 500–505.
62. Keramidas, A., Moorhouse, A. J., French, C. R., Schofield, P. R. & Barry, P. H. (2000). M2 pore mutations convert the glycine receptor channel from being anion- to cation-selective. *Biophys. J.* **79**, 247–259.
63. Gunthorpe, M. J. & Lummis, S. C. (2001). Conversion of the ion selectivity of the 5-HT(3a) receptor from cationic to anionic reveals a conserved feature of the ligand-gated ion channel superfamily. *J. Biol. Chem.* **276**, 10977–10983.
64. Corringer, J.-P., Bertrand, S., Galzi, J.-L., Devillers-Thiery, A., Changeux, J.-P. & Bertrand, D. (1999). Mutational analysis of the charge selectivity filter of the α7 nicotinic acetylcholine receptor. *Neuron*, **22**, 831–843.
65. Kelley, S. P., Dunlop, J. I., Kirkness, E. F., Lambert, J. J. & Peters, J. A. (2003). A cytoplasmic region determines single channel conductance in 5-HT3 receptors. *Nature*, **424**, 321–324.
66. Eisele, J.-L., Bertrand, S., Galzi, J.-L., Devillers-Thiery, A., Changeux, J.-P. & Bertrand, D. (1993). Chimaeric nicotinic-serotonergic receptor combines ligand binding and channel specificities. *Nature*, **366**, 479–483.
67. Devillers-Thiery, A., Giraudat, J., Bentaboulet, M. & Changeux, J.-P. (1983). Complete mRNA coding sequence of the acetylcholine binding α-subunit of *Torpedo marmorata* acetylcholine receptor: a model for the transmembrane organization of the polypeptide chain. *Proc. Natl Acad. Sci. USA*, **80**, 2067–2071.
68. Tierney, M. L., Osborn, K. E., Milburn, P. J., Stowell, M. H. B. & Howitt, S. M. (2004). Phylogenetic conservation of disulfide-linked, dimeric acetylcholine receptor pentamers in southern ocean electric rays. *J. Expt. Biol.* **207**, 3581–3590.
69. Nomoto, H., Takahashi, N., Nagaki, Y., Endo, S., Arata, Y. & Hayashi, K. (1986). Carbohydrate structures of acetylcholine receptor from *Torpedo californica* and distribution of oligosaccharides among the subunits. *Eur. J. Biochem.* **157**, 233–242.
70. Yonekura, K., Maki-Yonekura, S. & Namba, K. (2003). Complete atomic model of the bacterial flagellar filament by electron cryomicroscopy. *Nature*, **424**, 643–650.
71. Brunger, A. T., Adams, P. D., Clore, G. M., DeLano, W. L., Gros, P., Grosse-Kunstleve, R. W. *et al*. (1998). Crystallography and NMR system: a new software suite for macromolecular structure determination. *Acta Crystallog. sect. D*, **54**, 905–921.
72. Laskowski, R. A., MacArthur, M. W., Moss, D. S. & Thornton, J. M. (1993). PROCHECK: a program to check the stereochemical quality of protein structures. *J. Appl. Crystallog.* **26**, 283–291.
73. Kraulis, P. J. (1991). MOLSCRIPT: a program to produce both detailed and schematic plots of protein structures. *J. Appl. Crystallog.* **24**, 946–950.
74. Evans, S. V. (1993). SETOR: hardware lighted three-dimensional solid model representations of macromolecules. *J. Mol. Graph.* **11**, 134–138.

75. Nicholls, A., Sharp, K. & Honig, B. (1991). A rapid finite difference algorithm, utilizing successive overrelaxation to solve the Poisson–Boltzmann equation. *J. Comput. Chem.* **12**, 435–445.
76. Grutter, T. & Changeux, J.-P. (2001). Nicotinic receptors in wonderland. *Trends Biochem. Sci.* **26**, 459–463.

Edited by W. Baumeister

(Received 20 October 2004; received in revised form 9 December 2004; accepted 15 December 2004)